Three-dimensional steep wave impact on a vertical plate with an open rectangular section

Ioannis K. Chatjigeorgiou , Alexander A. Korobkin , Mark J. Cooker

PII: S0020-7403(17)31227-4
DOI: 10.1016/j.ijmecsci.2017.08.045
Reference: MS 3896

To appear in: *International Journal of Mechanical Sciences*

Received date: 9 June 2017
Revised date: 31 July 2017
Accepted date: 21 August 2017

Please cite this article as: Ioannis K. Chatjigeorgiou , Alexander A. Korobkin , Mark J. Cooker , Three-dimensional steep wave impact on a vertical plate with an open rectangular section, *International Journal of Mechanical Sciences* (2017), doi: 10.1016/j.ijmecsci.2017.08.045

Highlights

- The three-dimensional hydrodynamic slamming problem on a vertical plate subjected to the impact of a steep wave using linear potential theory is considered.
- The problem is complicated by assuming a rectangular opening on the plate.
- The examined configuration determines two boundary value problems with mixed conditions.
- The mathematical process assimilates the plate with a degenerate elliptical cylinder allowing the employment of elliptical harmonics.
- The mixed boundary value problems are tackled using robust mathematical analysis.
- The theory is extended to the computation of the total impulse exerted on the plate using pressure-impulse theory.

Three-dimensional steep wave impact on a vertical plate with an open rectangular section

Ioannis K. Chatjigeorgiou[1]
School of Naval Architecture and Marine Engineering, National Technical University of Athens, Greece
School of Mathematics, University of East Anglia, Norwich, UK

Alexander A. Korobkin
School of Mathematics, University of East Anglia, Norwich, UK

Mark J. Cooker
School of Mathematics, University of East Anglia, Norwich, UK

Abstract The present study treats the three-dimensional hydrodynamic slamming problem on a vertical plate subjected to the impact of a steep wave moving towards the plate with a constant velocity. The problem is complicated significantly by assuming that there is a rectangular opening on the plate which allows a discharge of the liquid. The analysis is conducted analytically assuming linear potential theory. The examined configuration determines two boundary value problems with mixed conditions which fully are taken into account. The mathematical process assimilates the plate with a degenerate elliptical cylinder allowing the employment of elliptical harmonics that ensure the satisfaction of the free-surface boundary condition of the front face of the steep wave, away from the plate. This assumption leads to an additional boundary value problem with mixed conditions in the vertical direction. The associated problem involves triple trigonometrical series and it is solved through a transformation into integral equations. To tackle the boundary value problem in the vertical direction a perturbation technique is employed. Extensive numerical calculations are presented as regards the variation of the velocity potential on the plate at the instant of the impact which reveals the influence of the opening. The theory is extended to the computation of the total impulse exerted on the plate using pressure-impulse theory.

Keywords: Steep wave impact; pressure-impulse; elliptical harmonics; mixed boundary value problems; triple trigonometrical series; integral equations.

[1] Corresponding author: Tel. +30 210 772 1105, Fax. +30 210 772 1412, email: chatzi@naval.ntua.gr

1 Introduction

It is crucial to know the effects of violent wave impact on structures that are built in or are operated in sea waves. We are concerned with the forces and flows which occur when waves break against structures such as harbour walls, moored or fixed offshore platforms and seagoing vessels in head seas. We focus on violent breaking wave impact and this should be distinguished from the effects induced by regular waves. Steep and breaking waves can exert forces many times greater than non-breaking waves such as standing waves adjacent to a monolithic vertical harbour wall. Standing waves have pressure and velocity fields that varying in a time-harmonic manner within a continuous dynamic process. By contrast, a violent wave impact is a discontinuous process in time, with a sudden collision between a volume of water in the incident breaking wave and the structure. The duration of the typically huge pressure associated with impact is very short, and the pressure exerts a huge short-lived net hydrodynamic load on the impacted structure. In order to form a mathematical theory of impact it is important to study and understand in detail the early stages of impact, when the largest hydrodynamic load occurs.

There are other facets of the problem that distinguish wave impact and make it particularly difficult to study. Much work has been done in theoretical and controlled experimental investigations in two space dimensions (2D). However, a major challenge, to bring the theory closer to realistic sea wave conditions, is to understand wave impact in three space dimensions (3D). The mathematical theory of breaking-wave impact involves satisfying nonlinear boundary conditions on a free surface. The position of the free surface is one of the unknowns of the problem, and it has to be found as part of the solution – it is a so-called free-boundary problem. The problems should be structured as boundary value problems with mixed conditions; so called Mixed Boundary Value Problems (MBVPs). An additional difficulty arises from the fact that in the general case of 3D wave impact, the impacted wetted region on the structure is one of the problem‟s unknowns, whose boundary should be determined, based on specific assumptions regarding the pressure and velocity of the liquid on the contact line where the free-surface meets the structure [1-3]. Nevertheless, we will not go pursue that discussion here as the theoretical model used in this paper requires the wetted region to be prescribed. Another difficulty is the nonlinear boundary conditions, and this aspect is simplified by using linearisations of the boundary conditions.

Judging from the published literature, wave impact has been studied theoretically much less than the class of problems associated with the entry of a body into initially static water – so called water-entry problems. In wave impact problems, the region of liquid that impacts the structure has free surfaces on two sides, the top surface of the wave and the steep wave front that hits the structure. In contrast, in water entry problems, which also lead to slamming, the single free surface has a simpler geometry. The more complicated shape and behaviour of the free surfaces during wave impact is harder to model than for a water-entry problem.

Clearly, the proper formulation of a wave impact problem should be set in 3D. The difficulties associated with 3D descriptions and the solution methodologies that should be followed, discourages investigation. In the review paper of Peregrine [4] the author recognises that „*In the three-dimensional world at the edge of an ocean, many aspects of the fluid dynamics may differ, so we reconsider some of our assumptions*‟. Nevertheless, the literature associated with analytical studies in wave impact problems has so far focused almost exclusively on 2D formulations and approximations, relevant to the geometric settings of the most violent impacts. The 2D theory has reached some maturity. Although they consider mainly impact on vertical walls, they have introduced additional model features that could make the results more realistic. In this context, Wood et al. [5] used pressure-impulse theory to investigate the effect of trapped air in breaking wave impact. Using the same method Wood and Peregrine [6] extended their work to study wave impact on a porous berm. Violent breaking wave impact was investigated in a series of papers by Bullock et al. [7] and Bredmose et al. [8-9]. Bullock et al. [7] presented experimental measurements of pressure from breaking wave tests on vertical and inclined walls. Brendmose et al. [8] considered the effect of the trapped air in the

cavity formed by a breaking wave, while in the last study of the same series of papers, Brendmose et al. [9] took into account possible aeration of the liquid. Cooker [10] studied the interaction of a breaking wave with a permeable vertical wall. Experiments on breaking wave impacts on vertical walls were performed by Cuomo et al. [11]. They generated waves that steepened due to a sloped bed that ran up to the wall. The shoaling conditions were arranged to ensure that the steepening of the waves led to impacts as close to 2D as possible. Examples of studies that rely on numerical methods to solve 2D problems of breaking wave on vertical walls are those due to Rafiee et al. [12] and Carratelli et al. [13]. Both studies apply the method of Smoothed Particle Hydrodynamics (SPH), a method that appears to be more flexible than other Computational Fluid Dynamics (CFD) solvers for impact problems.

An important simplification is to treat the face of the breaking wave as parallel to the wall at the instant of impact. For a vertical wall the wave front is considered everywhere vertical, thus ensuring maximum hydrodynamic load. In this context, Korobkin and Malenica [14] studied analytically steep wave impact on an elastic wall, and recently Noar and Greenhow [15] applied the steep wave impact concept to rectangular geometries using pressure-impulse theory. Again, both studies were conducted in 2D. For 2D wave impact problems involving non-classical boundary conditions, such as those determined by porous or perforated surfaces, see the short review paper of Korobkin [16].

By contrast, there are few studies in 3D and they have only employed numerical solvers. One method for generating a wave that collides violently with a structure is that of the so-called dam-break flow. That is, the wave generated by a liquid domain which originally is confined by a barrier and released suddenly. Examples of 3D studies on the subject are those due to Kleefsman et al. [17] and Yang et al. [18]. The former study applied a Volume-of-Fluid (VOF) method to simulate the impact of a dam-break flow on perfectly rectangular bodies. Yang et al. [18] used the unsteady Reynolds equations to simulate near-field dam-break flows, and to estimate the impact forces on obstacles. The cases considered resemble flood-like flows and they cannot be characterized as violent wave impact.

Dam-break flows have also been studied using Smoothed Particle Hydrodynamics (SHP) methodologies. Examples are the studies of Gómez-Gesteira and Dalrymple [19] and Cummins et al. [20] who examined the impact of a single wave, originating from a dam-break, with a tall coastal structure. In both studies, the structure was a vertical rectangular column. To the author‟s best knowledge, there have been no 3D studies, even using numerical methods, for more complicated convex geometries, such as circular cylinders. The main difficulty arises from the fact that the impacted wetted region is not known explicitly and must be treated as one of the problem‟s unknowns. Clearly, relevant difficulties are not encountered when the impacted structure is rectangular with the front face of the wave parallel to one of the plane vertical faces of the rectangular column. It is evident that in this case the boundary of the region hit by the wave is known in advance. The same is true for the contact lines between the liquid and the body, as these coincide with the column‟s vertical edges.

The present study is a contribution towards 3D approaches on wave impact problems. The physical scenario is a vertical plate, which is subjected to impact by a steep wave which before impact was propagating towards the plate with a constant uniform velocity. The problem is complicated by assuming that the plate has a rectangular opening. The opening (or gap) extends horizontally to the vertical edges of the plate. The positions of the upper and lower edges of the rectangular gap are fixed in time, and we investigate the influence of different positions. At impact the liquid facing the gap is free to discharge through it. Our aim is to find the influence of the gap dimensions on the total force on the structure and the sudden flow through the gap. There are several motivations for having a gap in the plate. One is to extend our earlier work [21] with a single rectangular plate, to treat more realistic structures that may be cracked or contain a designed slot. Another context is a plunging wave impact that captures a thin bubble of constant-pressure air adjacent to the structure, in which of the forward face of the wave is in contact with the structure only above and below the air pocket.

Mathematically, the complexity of the problem originates from the fact that two mixed boundary value problems (MBVP) should be considered in the two directions of the forward face of the wave. To solve simultaneously both problems, the plate is approximated by a degenerate elliptical cylinder with zero semi-minor axis. Having properly formulated one of the two MBVPs, the second (in the vertical direction) yields a one-dimensional MBVP involving triple trigonometric series. It should be mentioned that in contrast to dual trigonometric series, triple series have been only a little studied. The solution provided is based on the transformation of the triple trigonometric series into triple series of integral equations. The solution method allows the derivation of analytical expressions for the velocity potential. One goal is to arrive at expressions that relate the 3D solution to 2D approximations. A second goal of the work is to use pressure-impulse theory to estimate the total impulse on the plate due to the impact.

The study is structured as follows: in Section 2 we formulate the hydrodynamic problem and describe the solution method employed to account for the mixed conditions in the horizontal direction. The solution method relies on the expansion of the velocity potential in elliptical harmonics, as products of the radial and periodic Mathieu functions. Section 3 contains expansions in perturbations to formulate the triple trigonometrical series MBVP. That problem is further analyzed in Section 4. In Section 5 the associated MBVP is transformed into a MBVP involving integral equations. The method of solution relies on the reduction of the triple series into a dual series. That is achieved in Section 6. Section 7 is dedicated to the solution of the dual series. Section 8 applies pressure-impulse theory to calculate the total impulse exerted on the plate. Relevant computations are presented in Section 8 followed by a discussion. Finally, the conclusions of the study are presented in Section 9.

2 The hydrodynamic problem

The fluid in the steep wave moves at constant velocity towards the plate that is situated at ώ = π (Fig. 1). The fluid domain is part of ώ ≤ π. The width of the plate is ςϋ and the water depth is constant and equal to ΄Ο. A Cartesian coordinate system is defined with its origin fixed on the plate at ώ = π, in the centre line of the plate at ϋ = π and on the free-surface on ΰ = π. The ΰ-axis is pointing in the gravity direction and the flat bottom is situated on ΰ = ΄Ο. The plate has a rectangular opening with its horizontal edges located at ΰ = ΰ and ΰ = ΰ from the free-surface. The opening allows a discharge of the liquid at the time of impact. The thickness of the plate at ΰ ≤ ϋ ≤ ΰ and ϋ = ϋ is considered negligible.

The liquid is assumed to be inviscid and incompressible and the flow irrotational allowing the employment of the linear potential theory. The sudden change in the velocity potential at the instant of the impact is denoted by ϋ. We employ the small time approximation and we use nondimensional variables ΰ = ϋ ΰ, ϋ = ΰ ϋ, ΰ = ΰ ϋ, = ‰ϋ, ΄Ω = ΄Ο ϋ, ΰ = ΰ ϋ and ΰ = ΰ ϋ. Accordingly, the flow will be described (in nondimensional variables) through the following MBVP (see also Fig. 1).

$$\nabla \cdot \% = \pi \qquad \text{in } \Omega \qquad (1)$$

$$\% = \pi \qquad \text{on } \Gamma_F \qquad (2)$$

$$\% = \pi \qquad \text{on } \Gamma_P \cup \Gamma_B \qquad (3)$$

$$\frac{\partial \%}{\partial \eta} = \pi \qquad \text{on } \Gamma_F \qquad (4)$$

$$\frac{\partial \%}{\partial \nu} = \rho \qquad \text{on } \Gamma_P \cup \Gamma_B \qquad (5)$$

‰ سي πℏ ώ سي πℏ ʂώʂ حى ρℏ ῶ حى ᾳ حى ῶ ℏ (6)

‾ ‰ / ‾ ώ سي ρℏ ώ سي πℏ ʂώʂ حى ρℏ π حى ᾳ حى ῶ ℏ (7)

‰ ο πℏ ώ · ط ώ · ο Ⱨ℔ (8)

The field equation under the employed assumptions for the flow is the Laplace‟s equation (1). The boundary conditions of Eqs. (2), (3) and (6) follow from the linearized dynamic conditions on the free-surfaces and the initial conditions that before the impact the fluid moves towards the plate with spatially uniform velocity طώ. The function ‰ ώℏώℏᾳ is the sudden change in the velocity potential, consistent with the fluid remaining in contact with the plate after the impact. The condition (2) applies on the upper free-surface and condition (3) refers to the front face of the steep wave, to the left and the right of the impacted area. Condition (6) is the linearized condition on the rectangular opening through which the liquid is discharged. Also, Eq. (4) is the kinematic condition on the flat horizontal bottom, while Eqs. (5) and (7) follow from the condition that the liquid hits the plate, does not penetrate it and remains in sliding contact with the impermeable upper and lower sections of the plate. Finally, Eq. (8) is the far-field condition which indicates that the disturbance, due to the impact, vanishes at infinity. The model Eqs. (1)-(8) contain geometric parameters ῶ and ῶ to specify the position and the width of the gap in the plate, and the depth Ω which we suppose is small enough (compared with the unit width of the plate) for certain expansions below to converge.

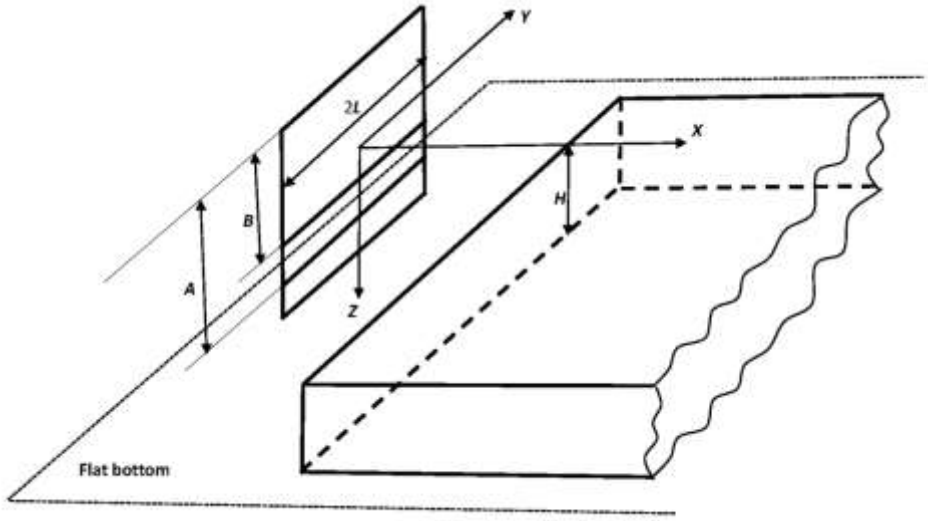

Fig. 1 The geometry of the impact problem.

To satisfy the system of Eqs. (1)-(8), and to find an analytical solution to the linearized problem, we start by considering the following form for the velocity potential

‰ ώℏώℏᾳ سي ∞ ‰ح ώℏώ ÓÉÎ ₌حᾳ ℏ (9)
ح=١

where ₌ح سي è طي ρjς “ jΩ. Equation (9) satisfies the kinematic condition on the horizontal bottom [Eq. (4)] and the dynamic condition on the upper free-surface [Eq. (2)]. Equation (9) originates from the employment of the method of separation of variables for the solution of the Laplace equation (1). It literarily expresses the linear superposition of the modal solutions of the Laplace equation. Given that the vertical variation of the velocity potential ‰ ώℏώℏᾳ is explicitly described through ÓÉÎ ₌حᾳ , which additionally satisfy the boundary conditions (2) and (4), the next step is to calculate the modal plane potentials ‰ح ώℏώ .

Substituting Eq. (9) into the Laplace equation (1) shows that the functions $\phi_n(\xi)$ satisfy the two-dimensional Helmholtz equation

$$\frac{\partial^2 \phi_n}{\partial \xi^2} + \frac{\partial^2 \phi_n}{\partial \eta^2} + k^2 \phi_n = 0 \tag{10}$$

The solution for ϕ or equivalently ϕ_n, should take into account the boundary condition (3) on the outer parts of the front face of the steep wave. Noting that a plate with finite dimensions can be effectively represented by an elliptical cylinder with zero semi-minor axis, we transform the Helmholtz equation using elliptical coordinates (ξ, η), with

$$x = f \cosh\xi \cos\eta \tag{11}$$

$$z = f \sinh\xi \sin\eta \tag{12}$$

The elliptical coordinates ξ = constant, η = constant are orthogonally intersecting families of confocal ellipses and hyperbolae, respectively, while f is the half distance between the foci and is related with the semi-major and semi-minor axes of the elliptical cylinder a, b respectively by $f = \sqrt{a^2 - b^2}$. The elliptical cylinder approximates a plate assuming $b = 0$ and in nondimensional form $f/a = \rho$. The surface of the plate is determined by $\xi_p = \mathrm{ARCOSH}(1/\rho)$, $-\pi < \eta \le \pi$.

Next, in elliptical coordinates, Eq. (10) becomes

$$\frac{1}{f^2(\cosh^2\xi - \cos^2\eta)} \left(\frac{\partial^2 \phi_n}{\partial \xi^2} + \frac{\partial^2 \phi_n}{\partial \eta^2} \right) + k^2 \phi_n = 0 \tag{13}$$

Note that the plane Laplace operator in Cartesian representation $\partial^2/\partial x^2 + \partial^2/\partial z^2$ is transformed in elliptic coordinates as $1/f^2(\cosh^2\xi - \cos^2\eta)\left(\partial^2/\partial\xi^2 + \partial^2/\partial\eta^2\right)$. Assuming separable solutions, the component $\phi_n(\xi, \eta)$ that satisfies Eq. (13) is expanded in terms of elliptical harmonics as

$$\phi_n(\xi,\eta) = \sum_{m=0}^{\infty} \left[A_m^{(1)} \mathrm{Ce}_m(\eta, q) + B_m^{(1)} \mathrm{Se}_m(\eta, q) \right] \left[C_m^{(1)} \mathrm{Ce}_m(i\xi, q) + D_m^{(1)} \mathrm{Se}_m(i\xi, q) \right]$$
$$+ \sum_{m=0}^{\infty} \left[A_m^{(2)} \mathrm{Ce}_m(\eta, q) + B_m^{(2)} \mathrm{Se}_m(\eta, q) \right] \left[C_m^{(2)} \mathrm{Ce}_m(i\xi, q) + D_m^{(2)} \mathrm{Se}_m(i\xi, q) \right] \tag{14}$$

where Ce_m and Se_m denote the even and odd periodic Mathieu functions, while Ce_m and Se_m are the even and odd modified (radial) Mathieu functions in the notation of Abramowitz and Stegun [22]. The superscript labels (1) and (3) designate the kind of the radial Mathieu functions. Finally, $q = -k^2 f^2/4$ and it is noted that the separation constant involved in the elliptical harmonics (the so-called Mathieu parameter), is negative.

The boundary conditions of Eqs. (3) and (8), expressed in terms of the expansions in elliptical harmonics $\phi_n(\xi, \eta)$ will read

$$\phi_n(\xi, -\pi) = \phi_n(\xi, \pi) \tag{15}$$

$$\phi_n(\xi, \eta) = -\pi/2 \qquad \xi = \xi_p \tag{16}$$

Of the radial functions present in Eq. (14), only the Mathieu functions of the third kind satisfy the far-field condition of Eq. (8). Accordingly the products that involve $\ddot{w}_{\zeta}^{\circ}$ and $\dot{i}_{\zeta}^{\circ}$ are omitted. In addition, the conditions of Eq. (15) are satisfied only by the odd periodic Mathieu functions $i\Omega_{\zeta}$ $\dot{u}_{\eta}$. Lastly, it is remarked that the velocity potential is defined in the half plane $u > -\pi$ and as a result only the odd terms $\alpha_{s} \cos(s\eta)$ should be retained. Hence, Eq. (14) is simply

$$\phi_{c} = \sum_{s=1}^{\infty} A_{s}^{(c)} \dot{i}_{s}^{(1)} i\Omega_{s} \dot{u}_{s} \tag{17}$$

where the odd periodic Mathieu function can be written as a Fourier series

$$i\Omega_{s} \dot{u}_{s} = \sum_{r=1}^{\infty} B_{r}^{(s)} \sin(r\eta) \tag{18}$$

In Eq. (18) the constants $B_{r}^{(s)}$ for $B_{r}^{(s)}$ are the expansion coefficients of the odd periodic Mathieu functions $i\Omega_{s} \dot{u}_{s}$.

The total velocity potential will read

$$\phi = \sum_{s=1}^{\infty} \sum_{r=1}^{\infty} A_{s}^{(c)} \dot{i}_{s}^{(1)} i\Omega_{s} \dot{u}_{s} \sin(r\eta) \tag{19}$$

The unknown expansion coefficients $A_{s}^{(c)}$ are determined by applying the remaining boundary conditions of Eqs. (5)-(7). The tilde above A will be dropped in the sequel.

The boundary conditions of Eqs. (5)-(7) expressed in elliptical coordinates become

$$\frac{\partial \phi}{\partial \xi} = \frac{\partial \Omega}{\partial t} \quad \text{at} \quad \xi = \xi_{0}, \quad \eta \in [-\pi, \pi] \tag{20}$$

$$\phi = \phi_{0} \quad \text{at} \quad \xi = \xi_{0}, \quad \eta \in [-\pi, \pi] \tag{21}$$

$$\frac{\partial \phi}{\partial \xi} = \frac{\partial \Omega}{\partial t} \quad \text{at} \quad \xi = \xi_{0}, \quad \eta \in [-\pi, \pi] \tag{22}$$

Next, we substitute the velocity potential from Eq. (19) into the boundary conditions of Eqs. (20)-(22) to obtain

$$\sum_{s=1}^{\infty} \sum_{r=1}^{\infty} A_{s}^{(c)} \dot{i}_{s}^{(1)} i\Omega_{s} \dot{u}_{s} \sin(r\eta) = \sum_{s=1}^{\infty} B_{s}^{(c)} \dot{i}_{s}^{(1)} \dot{u}_{s} \cos(s\eta) \cos(r\eta) \tag{23}$$

$$\sum_{s=1}^{\infty} \sum_{r=1}^{\infty} A_{s}^{(c)} \dot{i}_{s}^{(1)} i\Omega_{s} \dot{u}_{s} \sin(r\eta) = \phi_{0} \tag{24}$$

where the prime denotes differentiation with respect to the first argument. Both Eqs. (23) and (24) are defined in the interval $-\pi < \eta < \pi$. It is noted that $\dot{i}_{s}^{(1)} \dot{u}_{s}$ is given by Abramowitz and Stegun [22; Eqs. (20.8.9) and (20.8.11)]

$$[illegible] \quad (25)$$

where [illegible] and [illegible] denote the modified Bessel functions of the first and the second kind respectively, [illegible], [illegible] and [illegible] are the expansion coefficients of the even periodic Mathieu functions [illegible]. These are given by

$$[illegible] \quad (26)$$

while it holds that [22; Eq. (20.8.4)]

$$[illegible]$$

Letting [illegible] in Eq. (25) it can be shown that

$$[illegible] \quad (27)$$

For the derivation of Eq. (27) the Wronskian determinant for Bessel functions was used [22; Eq. (9.6.15)]. The corresponding expression for the derivative of the radial Mathieu function as [illegible] is more complicated and is given by

$$[illegible] \quad (28)$$

In the case of a solid rigid plate without an opening, the body condition is described solely by Eq. (23) defined in the intervals [illegible] and [illegible]. Hence, employing orthogonality of the involved eigenfunctions, the expansion coefficients [illegible] are

$$[illegible] \quad (29)$$

and the velocity potential [illegible], calculated exactly on the plate at [illegible] from Eq. (19) is given by

$$[illegible] \quad (30)$$

Equation (30) is valid for any aspect ratio [illegible]. Also, Eq. (30) can provide the 2D strip theory solutions with vertical or horizontal strips assuming a very wide plate, [illegible] 1, [illegible], or a very narrow plate, [illegible]. Here we are interested in only relatively wide plates and therefore further analysis assuming [illegible] is omitted. Taking the asymptotics of the derivative of the radial

Mathieu function for very large Mathieu parameters which implies taking the asymptotics of the Bessel functions (and their derivatives) for very large arguments [see also Eq. (28)] it can be shown that

$$[illegible] \tag{31}$$

Using Eqs. (27) and (31), Eq. (30) becomes

$$[illegible] \tag{32}$$

Assuming that the term in square brackets equals some function [illegible], then we can apply the orthogonality relation of [illegible] for [illegible]. This gives

$$[illegible] \tag{33}$$

The left hand side of Eq. (33) equals [illegible]. Hence, by comparing with Eq. (18) the identity (33) holds if and only if [illegible]. The 2D solution is obtained by letting [illegible] and eventually Eq. (32) becomes

$$[illegible] \tag{34}$$

Equation (34) is explicitly identical with the 2D strip theory solution [illegible] provided by King and Needham [23].

We now revert to the actual 3D problem, which has been reduced to Eqs. (23) and (24). These equations represent a MBVP defined only in the vertical direction. In fact, Eqs. (23) and (24) represent a triple trigonometrical series. Analytical solutions for relevant problems are feasible only if the unknown expansion coefficients that multiply the trigonometrical functions are the same. Here however, we treat a different, and more complicated case, as the coefficients of [illegible] in Eq. (23) depend on the derivative of the radial Mathieu function, whilst those of Eq. (24) depend on the Mathieu function itself. To address properly this challenge a more sophisticated approach should be taken, as described in the next section.

3 Expansion of the derivative of the radial Mathieu function in a series of perturbations

Equation (28) is further elaborated using the series expansions of the modified Bessel functions that can be found in [22; Eqs. (9.7.1) – (9.7.4)]. In particular it holds that

$$[illegible] \tag{35}$$

$$[illegible] \tag{36}$$

$$\text{[illegible]} \quad (37)$$

$$\text{[illegible]} \quad (38)$$

where [illegible]. Substituting Eqs. (35)-(38) into Eq. (28) and performing lengthy algebraic manipulations, it can be shown that the [illegible] term of the components within the square brackets of Eqs. (35)-(38) vanish. Overall Eq. (28) can be written as

$$\text{[illegible]} \quad (39)$$

Defining [illegible], Eq. (39) can be written as

$$\text{[illegible]} \quad (40)$$

where we define

$$\text{[illegible]} \quad (41)$$

The second term in the right had side of Eq. (40) is negligible only if [illegible] is considered sufficiently large allowing the employment of the asymptotic formulae of the modified Bessel functions and their derivatives for very large arguments. In the present physical problem, that corresponds to the case of a relatively wide plate with small aspect ratio. The inclusion of that term in Eq. (40) extends the interval of convergence of that equation. Clearly, if additional accuracy is required one could include the [illegible] terms in Eqs. (35)-(38). The perturbation technique dictates that we must have all [illegible], in order to be able to enhance Eq. (40) with terms of order equal or higher than [illegible]. In fact [illegible] decreases to zero rapidly as [illegible] increases. Nevertheless, the requirement [illegible] should be valid for all [illegible], even the first one. That leads to the requirement [illegible].

The form obtained for the radial Mathieu function [see Eq. (40)] suggests taking the following expansion for the coefficients [illegible] [see Eqs. (23) and (24)]

$$\text{[illegible]} \quad (42)$$

Next, substituting Eqs. (40) and (42) into Eqs. (23) and (24) and equating like powers of [illegible] we obtain the following systems at orders [illegible] and [illegible] :

Order [illegible] :

$$\text{[illegible]} \quad (43)$$

[illegible] (44)

Order [illegible] :

[illegible] (45)

[illegible] (46)

where

[illegible] (47)

and

[illegible] (48)

The two orders of [illegible] will be referred in the sequel as the leading order and the first-order. Clearly, the solution of the first-order problem of Eqs. (45) and (46) dictates the solution of the problem at leading order [Eqs. (43) and (44)]. Both problems can be treated in a similar fashion. They are in fact single-dimensional boundary value problems of mixed type, involving triple trigonometrical series.

For the leading order problem it is observed that the MBVP of Eqs. (43) and (44) suggest assuming that the unknown expansion coefficients [illegible] are directly proportional to [illegible], and be written as [illegible], where [illegible] are constants. Therefore the solution of the associated triple trigonometrical series will provide sets of coefficients, not functions of [illegible] Those functions are simply obtained by the direct multiplication of the leading order constant expansion coefficients by [illegible]. Nevertheless, here we have chosen to follow a global notation for both triple trigonometrical series problems (at the leading and the first-order). Hence, the analysis that is conducted in the following will concern [illegible] as general functions of [illegible].

4 Mixed boundary value problems involving triple trigonometrical series

Boundary value problems of mixed type have many substantial applications, which aside from hydrodynamics involve rolling mechanics, electrostatics, thermoelasticity etc. (e.g. [24-26]). Here we consider a special case of mixed boundary value problems, those which involve trigonometrical series. Although mixed boundary value problems leading to dual trigonometrical series are well treated in the literature, there are only a few studies on triple trigonometrical series. The first solution to dual series was given by Shepherd [27]. Analytical solutions have been given by Tranter [28-30]. Srivastav [31] showed that certain dual trigonometrical relations can be reduced to a Fredholm integral equation of the second kind and, under specific conditions, can admit closed form solutions.

Studies approaching the analytic solution of triple trigonometrical series are scarce. For example the classic book of Sneddon [32] has references only on dual series, the book of Fabrikan [33] doesn‟t mention dual or triple trigonometrical series, while the last book on the subject by Duffy [34], has

only one specific example on sine series. Examples on triple trigonometrical series are the studies of Tranter [35] and Kerr et al. [36]. Tranter [35] showed that the solution of triple trigonometrical series can be sought by solving an equivalent system of three integral equations. Tranter‟s [35] work however is incomplete because although he considered both sine and cosine series involving harmonics ÓÉÎ ἑ طي ρjς – and ÃÏÓ ἑ طي ρjς – , π جى – جى “, he did not consider the case when the argument ἑ طي ρjς that multiplies the expansion coefficients is reversed. In fact, this is exactly the case that should be treated herein.

We start by considering the leading order problem of Eqs. (43) and (44) and we employ the following transformations: ʊ سي “ἀj ῭Ωἅ ὤₒ سي “ὤj ῭Ω and ὤₒ سي “ὤj ῭Ω. Further, making use of the orthogonality of ÓÉÎ ἑ طي ρjς ʊ , we approximate ÓÉÎ ὺ by

ÓÉÎ ὺ سي ÓÉÎ ὺ ς/“ همج ἑ طي ρjς ٩٥ ÓÉÎ ἑ طي ρjς ʊ ἅ π حى ʊ حى “ 8 (49)

We now define

Ὀح ٍ ὺ سي Ὀح ٍ ὺ طي ς/“ ἑ طي ρjς ٩٥ ÓÉÎ ὺἅ (50)

and Eqs. (43) and (44) are recast into the following pair of equations:

همج Ὀح ٍ ὺ ÓÉÎ ἑ طي ρjς ʊ سي πἅ π حى ʊ حى ὤₒἅ ὤₒ حى ʊ حى “ ἅ (51)

همج ἑجي طي ρ/ς ٩٥ Ὀح ٍ ὺ ÓÉÎ ἑ طي ρjς ʊ سي ῍Ο ٍ ὺἅʊ ἅ ὤₒ حى ʊ حى ὤₒ ἅ (52)

in which

῍Ο ٍ ὺἅʊ سي طي ς/“ ÓÉÎ ὺ همج ÓÉÎ ἑ طي ρjς ʊ / ἑ طي ρjς · 8 (53)

We choose to use a uniform expression for both ῍Ο ٍ ὺἅʊ and ῍Ο ٥ ὺἅʊ writing them as

῍Ο ج ὺἅʊ سي طي ς/“ همج ὠح ج ὺ ÓÉÎ ἑ طي ρjς ʊ ἅ ῍Ω سي πἅρἅ (54)

where

ὠح ٍ ὺ سي ἑ طي ρjς · ÓÉÎ ὺ (55)

and using Eq. (48)

ὠح ٥ ὺ سي طي ῍Ω·/ς“ همج ἑجي طي ρ/ς ٩١ طيρ جγ· ح ٍ γ· ح ὤ῍Ω· “/ς طي ὺἅ ήح 8 (56)

With these remarks we realize that the first-order problem is reduced to exactly the same form as the leading order problem, described through Eqs. (51) and (52), after replacing the index (0) by the index (1), using Ό ͦ ὺ سي Ό ͦ ὺ and taking ῎Ό ͦ ὺ῀ ἀ ḳ ῎Ό ͦ ὺ῀ ʊ from Eqs. (54) and (56).

5 Transformation of the trigonometrical series into a system of integral equations

Following the work of Williams [37], the idea of solving MBVPs involving triple trigonometrical series through transformation into integral equations was inspired by Tranter [35]. However, Tranter [35] considered only cases where in the intermediate interval, here indicated by ὥ حى ʊ حى ὥ, the multipliers of trigonometrical functions (both sine and cosine) have the form ἐ طي ρ j ς Ό. Although that seems insignificant, it does not allow the employment of Tranter‟s [35] method that was based on the Jacobi‟s expansion in a series of Bessel coefficients [38; p. 22].

To reform the triple trigonometrical series of Eqs. (51) and (52) into a system of triple integral equations we employ the transformation ϧ سي ÓÉÎ ʊ j ς ῀ʊ سي ς ÓÉÎ ϧ and we use the following useful relations that can be found in Gradshteyn and Ryzhik [39; p.717 and p.727]:

ÓÉÎ ςἐ طي ρ ÓÉÎ ϧ سي ρ طي ϧ ὺ ÓÉÎ ϧὸ Ώὸ῀ (57)

ρ / (ςἐ طي ρ) ÓÉÎ ςἐ طي ρ ÓÉÎ ϧ سي ὸ ὺ ÓÉÎ ϧὸ Ώὸ (58)

Using Eqs. (57) and (58), the system of Eqs. (51) and (52) yields for Ώ سي π῀ρ῀

Ό ὺ ὺ ὸ ÓÉÎ ϧὸ Ώὸ سي π῀ π حى ϧ حى ὥ῀ ὥ حى ϧ ῀ (59)

Ό ὺ ὸ ὺ ὸ ÓÉÎ ϧὸ Ώὸ سي ρ/ς ῎Ό ὺ῀ ς ÓÉÎ ϧ ῀ ὥ حى ϧ حى ὥ ῀ (60)

where ὥ سي ÓÉÎ ὥ j ς and ὥ سي ÓÉÎ ὥ j ς .

Accordingly, using Abramowitz and Stegun [22; Eqs. (10.1.1) and (10.1.11)]

ÓÉÎ ϧὸ سي “ϧὸ / ς ὺ ϧὸ ῀ ‘ سي ρ j ς (61)

and assuming

῎Ό ὺ῀ὸ سي Ό ὺ ὺ ὸ ῀ (62)

the system of Eqs. (59) and (60) finally becomes

ὸ ῎Ό ὺ῀ὸ ὺ ϧὸ Ώὸ سي π῀ π حى ϧ حى ὥ῀ ὥ حى ϧ ῀ (63)

$$\int_0^{\infty} \xi^{\nu+1} J_{\nu}(\xi r) \, d\xi \int_0^{\infty} \frac{\rho}{\zeta} \sin(\zeta z) \, d\zeta = \frac{r^{\nu}}{2^{\nu} \Gamma(\nu+1)} \int_0^{\infty} \zeta^{\nu+1} J_{\nu}(\zeta r) \, d\zeta \int_0^{\infty} \rho^{2\nu+1} \left(\rho^2 + z^2\right)^{-1} d\rho \qquad (64)$$

The system of Eqs. (63) and (64) is usually referred in the literature as a system of *Titchmarsh* type [40].

6 Transformation of the triple integral equations into dual trigonometrical series

Systems like Eqs. (63) and (64) are usually processed by attempting to satisfy by default one of the involved equations in a specific interval and then substituting the assumed solution into the remaining relations. Our procedure exploits the following integral relation [41; equation (3)], [38; p.401]

$$\int_0^{\infty} \xi^{\nu+1} J_{\nu}(\xi r) \, d\xi = \frac{2^{\nu} \Gamma(\nu+1)}{r^{\nu+1}} \qquad (65)$$

for $\nu > -1$ and $r > 0$.

For $z = 0$ the integral yields nonzero values and in particular

$$\int_0^{\infty} \xi^{\nu+1} J_{\nu}(\xi r) \, d\xi \int_0^{\infty} \frac{\rho}{\zeta} \sin(\zeta z) \, d\zeta = \frac{2^{\nu} \Gamma(\nu+1)}{r^{\nu+1}} \int_0^{\infty} \rho^{2\nu+1} \left(\rho^2 + z^2\right)^{-1} d\rho = \frac{\Gamma(\nu+1)}{r^{\nu+1}} \int_0^{\infty} \frac{\rho^{2\nu+1}}{\rho^2 + z^2} \, d\rho \qquad (66)$$

$$\int_0^{\infty} \xi^{\nu+1} J_{\nu}(\xi r) \, d\xi \int_0^{\infty} \frac{\rho}{\zeta} \sin(\zeta z) \, d\zeta = \frac{2^{\nu} \Gamma(\nu+1)}{r^{\nu+1}} \int_0^{\infty} \rho^{2\nu+1} \left(\rho^2 + z^2\right)^{-1} d\rho = \frac{\Gamma(\nu+1)}{r^{\nu+1}} \int_0^{\infty} \frac{\rho^{2\nu+1}}{\rho^2 + z^2} \, d\rho \qquad (67)$$

where ${}_2F_1$ denotes the hypergeometric function. The integral that appears in Eqs. (66) and (67) is known as the Sonine-Schafheitlin integral [39; p.683, Eqs. (6.574.1) and (6.574.3)], [38; p.401, Eq. (2)], [35]. The convergence of the integrals of Eqs. (66) and (67) requires that $2\mu > -\lambda - 1$ when $\nu > -1$ and $2\mu > \lambda - 1$ when $\nu > -1$. These conditions are satisfied by default herein as $\mu > 0$.

Accordingly we assume the following form for the unknown function $\Phi(r,z)$:

$$\Phi(r,z) = \int_0^{\infty} \Omega(\xi) \, J_{\nu}(\xi r) \, d\xi \qquad (68)$$

while we let $\nu > -1$. Hence, substituting Eq. (68) into Eq. (63) and rearranging the summation and the integration the following is obtained

$$\text{[illegible]} \qquad (69)$$

which holds true for $\ddot{w}. = 0$ due to Eq. (65). Thus, we have satisfied one of the three integral equations and in particular the one which should be valid for $\ddot{w}. = 0$. Accordingly, Eq. (68) is substituted into the remaining two integral equations (63) and (64). By exploiting Eqs. (66) and (67) for $0 = \ddot{w}.$ and performing some brief algebraic calculations the following are derived:

$$\text{[illegible]} \qquad (70)$$

$$\text{[illegible]} \qquad (71)$$

where we used $0 = \ddot{w}. \acute{E}\hat{I} -$. Equations (70) and (71) can be simplified significantly by expressing the hypergeometric functions in terms of sinusoidal harmonics [22; Eqs. (15.1.15) and (15.1.16)]. In order to increase the interval, in which the independent variable is defined, to $\pi\hbar$ " we let $- = \bar{\jmath}\varsigma$. Assuming also that $\grave{e}\,\text{[illegible]}\,\rho\jmath\varsigma \neq \Omega_{\zeta}^{\zeta} \upsilon = \ddot{\omega}_{\zeta}^{\zeta} \upsilon$, Eqs. (70) and (71) finally become

$$\text{[illegible]} \qquad (72)$$

$$\text{[illegible]} \qquad (73)$$

where $\Omega^{z} = \varsigma\ddot{\delta}.\jmath\ddot{w}..$

7 Solution of the dual trigonometrical series

7.1 Computation of the expansion coefficients of the dual trigonometrical series

Equations (72) and (73) form a one-dimensional MBVP that involves dual trigonometrical series. Systems of that kind are well treated in the literature and there have been several authors who provided complete solutions. For a summary the reader is referred to the classical book of Sneddon [29]. However, it should be mentioned that the suggested solutions were derived without being complemented by numerical computations. The solution provided in Sneddon [32] for instance, although accurate, does not allow efficient numerical evaluation as it requires the computation of the derivative of an integral for which no analytical solution exists and accordingly the only feasible way is to evaluate numerically. This type of complication is prone to numerical inaccuracies and accordingly the system of Eqs. (72) and (73) is treated further using the methodology suggested by Tranter [35].

By employing the transformations

$$\text{[illegible]}$$

the system of Eqs. (72) and (73) yields

[illegible] (74)

[illegible] (75)

The system of Eqs. (74) and (75) has been considered by Tranter [41] who found an appropriate way to employ Mehler‟s integrals [42; p. 52]. The solution provided (adapted in the present system) relies on the following recurrence relation for the computation of the expansion coefficients [illegible]:

[illegible] (76)

The remaining coefficient [illegible] is found by substitution of Eq. (76) into Eq. (74) for any value in the corresponding interval. For simplicity, this is chosen to be [illegible] Hence

[illegible] (77)

and the coefficients [illegible], [illegible] are obtained by the recurrence relation of Eq. (76).

In Eqs. (76) and (77), [illegible] denotes the Legendre polynomial with degree [illegible] and the prime denotes differentiation with respect to the argument. The derivative of the Legendre polynomials can be determined by the summation theorem [39; p.986]

[illegible] (78)

[illegible] (79)

where [illegible] can be any complex number.

The function [illegible] involved in Eqs. (76)-(77) is given by the elliptic integral

[illegible] (80)

or by evaluating the derivative with respect to [illegible]

[illegible] (81)

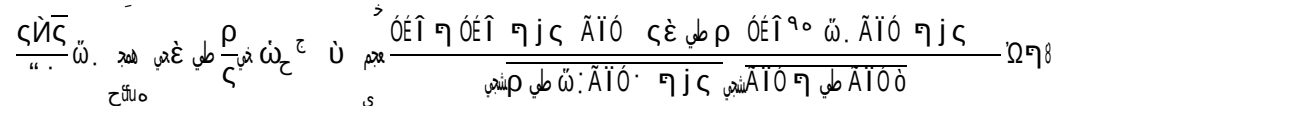

Although, the integral in Eq. (81) looks relatively complicated, it does not pose major difficulties in its numerical computation. In any event, it should be treated as an improper integral. As already mentioned, the solution at order $\varepsilon^{1/2}$ requires the solution at the leading order ε^{0}. In other words, one must obtain the original expansion coefficients $Y_{0}^{(0)}(x)$. Therefore the reversed procedure must be applied all the way to the very beginning to calculate the original expansion coefficients $Y_{0}^{(0)}(x)$. Nevertheless, this is not a simple straightforward process.

7.2 The reverse procedure

The reverse procedure could be applied at both orders ε^{0} and $\varepsilon^{1/2}$ to obtain the original coefficients of the Mathieu series expansions $Y_{0}^{(0)}(x)$, $\Omega = \pi/2$. Nevertheless, as it is discussed in the sequel, the computation of the leading order potential can be obtained directly through $f_{0}^{(0)}$ through Eq. (76) without the need to compute $Y_{0}^{(0)}(x)$. The latter however are required for the triple trigonometrical series problem at $\varepsilon^{1/2}$ due to the form of $O(\varepsilon^{1/2})$ given by Eqs. (54) and (56).

The reverse procedure requires us to start from $f_{0}^{(0)}$ and calculate sequentially $\tilde{\omega}_{0}^{(0)}$, $\Omega_{0}^{(0)}$, $O_{0}^{(0)}$, $O_{0}^{(0)}$ and finally $Y_{0}^{(0)}(x)$ through Eq. (47). Let us assume for the moment that we have been able to obtain $O_{0}^{(0)}$. Then the derivation of $Y_{0}^{(0)}(x)$ requires the employment of the orthogonality relation satisfied by the periodic Mathieu functions in Eq. (47). It is noted that $\mathrm{ce}_{2n}(\Omega x,\Omega^{2})$ (as well as the even periodic Mathieu functions) are orthogonal in the interval $[0,2\pi]$. The normalization constant is equal to π. Thus from Eq. (47) one obtains for $\Omega = \pi/2$

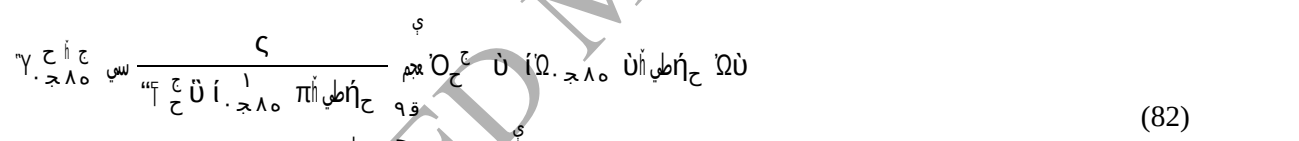

(82)

As already remarked in Section 3 the leading order coefficients $O_{0}^{(0)}$ [as well as all the leading order coefficients defined in the present: $f_{0}^{(0)}$, $\tilde{\omega}_{0}^{(0)}$, $\Omega_{0}^{(0)}$, $O_{0}^{(0)}$] are directly proportional to $\sin\theta$ and can be written as $O_{0}^{(0)} = \Theta_{0}^{(0)}\sin\theta$, where $\Theta_{0}^{(0)}$ are constants and they are the same coefficients as those calculated by the outlined procedure. Hence it is easily deduced that

(83)

The problem in the reversed procedure originates from the transformation of the trigonometrical series into integral equations. The turning point is Eq. (62) which together with Eq. (68) provide the identity

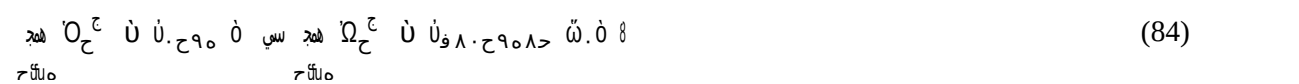

(84)

Assuming that the last coefficients we have calculated are those of the dual trigonometrical series of Eqs. (74) and (75), then we can easily see that $\Omega_{0}^{(0)} = \cos\theta\, f_{0}^{(0)}$. However, there is no

straightforward procedure to obtain ʹOح ͨ ὺ through ʹΩح ͨ ὺ using Eq. (84) and apparently the latter must be processed further.

Thus, we use again ﬤ سي ÓÉÎ ʊjς ὴʊ سي ςÓÉÎ ᵑᵒ ﬤ , π جى ﬤ جى ρ, π جى ʊ جى " and we multiply both sides of Eq. (84) by ÓÉÎ ﬤὸ . Accordingly we integrate in the semi-infinite interval πὴҔ to obtain

ﻫﻤﺢ ʹOح ͨ ὺ ﻌﺠﻢ ὺ.حᵑᵒ ὸ ÓÉÎ ﬤὸ ʹΩὸ سي ﻫﻤﺢ ʹΩح ͨ ὺ ﻌﺠﻢ ὺ.حᵑᵒ ὤ.ὸ ÓÉÎ ﬤὸ ʹΩὸ8 (85)

Note that ' سي ρjς and ὴ سي طي ρjς. We define '.حᵑᵒ ﬤ سي ὺ.حᵑᵒ ὤ.ὸ ÓÉÎ ﬤὸ ʹΩὸ which is calculated by [39; Eq. (6.6.71), p.17]

'.حᵑᵒ ﬤ سي πὴ ... (86)

Equation (86) implies that '.حᵑᵒ ﬤ سي π for ﬤ جي ὤ.. It can also be employed using ὤ. سي ρ. Therefore Eq. (84) yields

ﻫﻤﺢ ʹOح ͨ ὺ ÓÉÎ ὲ طي ρjς ʊ سي ﻫﻤﺢ ʹΩح ͨ ὺ ... 8 (87)

The derivation of Eq. (87) allows the employment of the orthogonality relation of ÓÉÎ ὲ طي ρjς ʊ in π جى ʊ جى ". Therefore the expansion coefficients ʹOح ͨ ὺ are found from ʹΩح ͨ ὺ through

ʹOح ͨ ὺ سي ... ʹΩʊ8 (88)

Having calculated ʹOح ͨ ὺ , the coefficients ʹOح ᵠ ὺ are given by Eq. (50), ʹOح ᵒ ὺ سي ʹOح ᵒ ὺ , while the original expansion coefficients will be obtained using Eq. (47).

8 Velocity potential and pressure-impulse

8.1 The velocity potential

The method of perturbations suggests taking the following form for the total velocity potential, calculated exactly on the surface of the plate for ό سي π

‰ πὴὺὴᾳ سي ‰ᵠ πὴὺὴᾳ طي ‰ᵒ πὴὺὴᾳ طي Ễ (89)

Accordingly, use of Eqs. (19), (40) and (42) requires that

$$\text{(90)}$$

$$\text{(91)}$$

The above are valid in the intervals $0 \le \xi \le \bar{\xi}_1$, $\bar{\xi}_2 \le \xi \le 1$, while the potentials should be zero in the intermediate interval $\bar{\xi}_1 \le \xi \le \bar{\xi}_2$. As a means for validating the present complicated method, we should verify that the potentials are indeed zero at the limiting points $\xi = \bar{\xi}_1$, $\xi = \bar{\xi}_2$. The curves of the potentials should be smooth and they should be zero at the above mentioned limiting points.

The numerical implementation of the theory outlined in the present requires some attention as regards the value of the aspect ratio Ω which in any case should be smaller than $\pi/2$. This can be traced back to the fact that the derivative of the radial Mathieu function was expanded in a series of perturbations and we retained only the leading order and the first-order terms of the series [see Eq. (40)]. Therefore for $\varepsilon \le \Omega \le \pi/2$ additional terms in the series of perturbations of Eqs. (42) and (89) might be required. Here, we present numerical results for two sufficiently small aspect ratios, $\Omega = 0.5$ and $\Omega = 0.8$ which accordingly ensure that all ε_n, $\varepsilon = 1,2,3,\ldots$ are sufficiently small allowing the approximation of the problem's parameters by only two terms of the perturbation expansion.

It is frequently stated that 3D effects in 3D impact problems are important close to the contact line between the body and the liquid. In the present case, it is anticipated that 3D effects will be important close to the edges of the plate at $\theta = \pm\alpha$. Relevant statements are usually provided without evidence on the variation of the 3D effects near to the contact line. The question which easily arises is, are 3D effects important close to the plate's edges and insignificant in the plate's vertical centreline? Also, given the fact that the potential is zero at the plate's edges, an additional question is where on the plate are 3D effects significant?

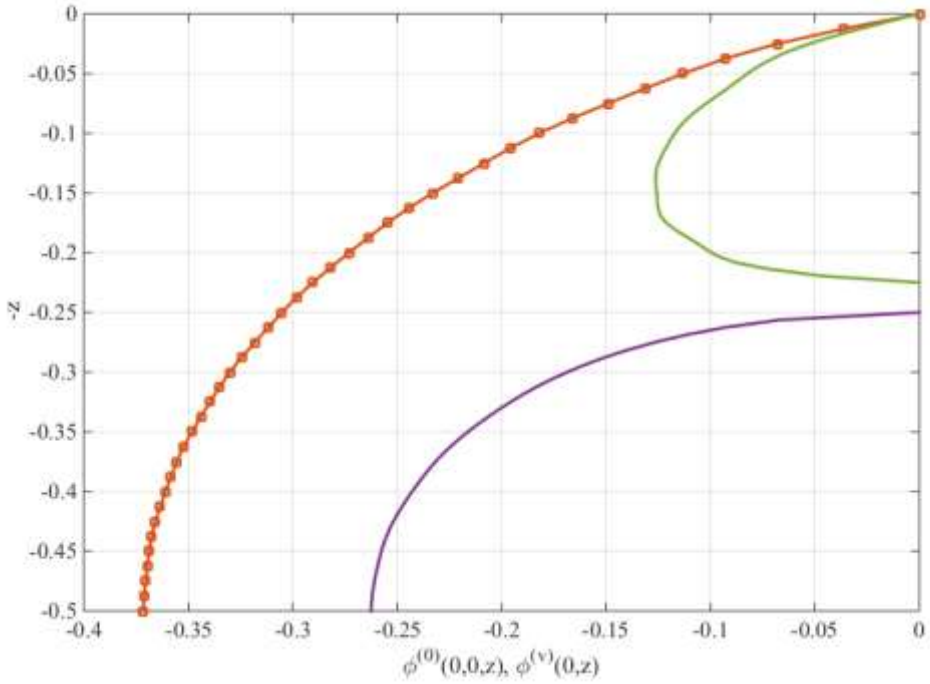

Fig. 2 The 2D strip theory solution (continuous red curve) compared with 3D solution (red symbols): ‴ سي ‴O j ‴ سي 0.5. For solving the MBVP it was assumed ‴ j ‴ سي 0.001, ‴ j ‴ سي 0.0001. The second case (green and purple curves) is for a wave impact on a plate with an open area in 0.45‴ حى ‴ حى 0.5‴

The solution provided by Eq. (34) is easily reproduced by the leading order potential of Eq. (90) (for ‴ سي π or ‴ طي سي “ j ς) as shown in Fig. 2. To obtain the results of Eqs. (34) through Eq. (90) we assumed an infinitesimal opening very close to the top of the plate, near the upper free-surface. Also, Fig. 2 depicts the velocity potential in the middle of the plate for a very small open area that was chosen to exist near the half of the plate‟s impacted height. The results are extremely interesting as they imply that if we allow the discharge of the liquid through a very small window, the velocity potential, and accordingly the pressure-impulse, on the two solid subsections are reduced substantially. The reason is that the velocity potential is forced to become zero at the horizontal edges of the open area. This finding has obvious significance for the design of coastal and offshore structures.

Figs. 3 and 4 show the behaviour of the velocity potential at the leading order and at the plate‟s centre line ‴ سي π, for a constant upper and lower edge respectively and increasing open area. The 2D solution with no gap [see Eq. (34)] is also shown as a reference. At the lower part of the plate the potential obtains its maximum at the bottom and progressively decreases to zero at the first horizontal edge from the bottom. In contrast, at the upper part of the plate the potential exhibits a parabolic behaviour having its maximum value near the middle of the upper part. Both figures show that an increase in the opening leads to a drastic decrease of the magnitudes of the velocity potential. In the part of the plate that maintains a constant height, the decrease of the potential appears not to be influenced by the surface of the opening.

The cases considered in Figs. 3 and 4 correspond explicitly to the middle of the plate. The 3D potential varies transversely (along ‴, or ‴) until it becomes zero at the plate‟s lateral edges. In fact the leading order potential ‰ ‹ πℓ‴ℓ‴ varies proportionally with ÓÉÎ ‴. This is better shown in the contour plots of Figs. 5-8 where the opening, in which the potential is zero, is immediately visible. All contour plots shown in the sequel depict the half-width of the plate due to symmetry. The axes lengths correspond to the aspect ratio ‴ being considered. As far as the leading order potential is concerned,

the 3D effects are explicitly described by the sinusoidal reduction from ù سي طي " j ς to ù سي π (and ù سي طي "). The pairs of Figs. 5-6 and 7-8 show that, overall, the magnitude of the velocity potential increases for increasing aspect ratio ΅ even though the normalized height and the position of the opening remain the same. The maxima of the leading order potential occur along the centreline of the contact region for ώ سي π. On the lower section the maxima are detected on the bottom, while on the upper section the strongest effect occurs close to its middle (with a very small shift towards the bottom).

We now discuss the leading order potential computed for several cases. From Figs. 5-8 we conclude that reducing the width of the gap increases the local maxima in potential on the upper and the lower sections of the plate. The increase in potential is associated with increased gradient in ‰, especialy at the edges of the plate section. These consequences suggest a higher fluid velocity, after impact, in the gap near its upper and lower boundaries. Comparing Figs. 5, 7 and 6, 8 it is easily deduced that allowing larger volume of liquid to pass through the opening on the plate, results in reduced impact effects, quantified by the velocity potential. The results due to the impact are mitigated not only because the contact region is reduced, but also because the velocity potential is decreased accordingly. An additional characteristic of the leading order potential, which should be highlighted, is related to its smooth variation in both directions ώℏά . By contrast, the first-order component of the potential is much more complicated and we discuss this next.

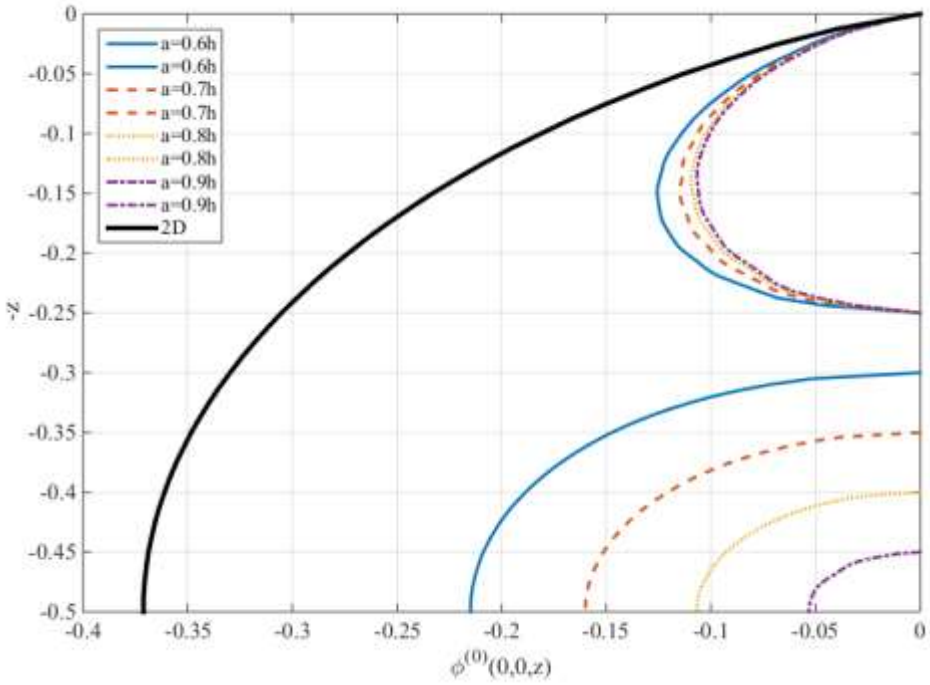

Fig. 3 The leading order potential ‰ ς πℏπℏά for a fixed upper edge ώ̃ j ΅ سي 0.5 and variable position of the lower edge ώ̈ΓΩ. The aspect ratio of the plate is ΅ سي ΅̈Ο j ü سي 0.5.

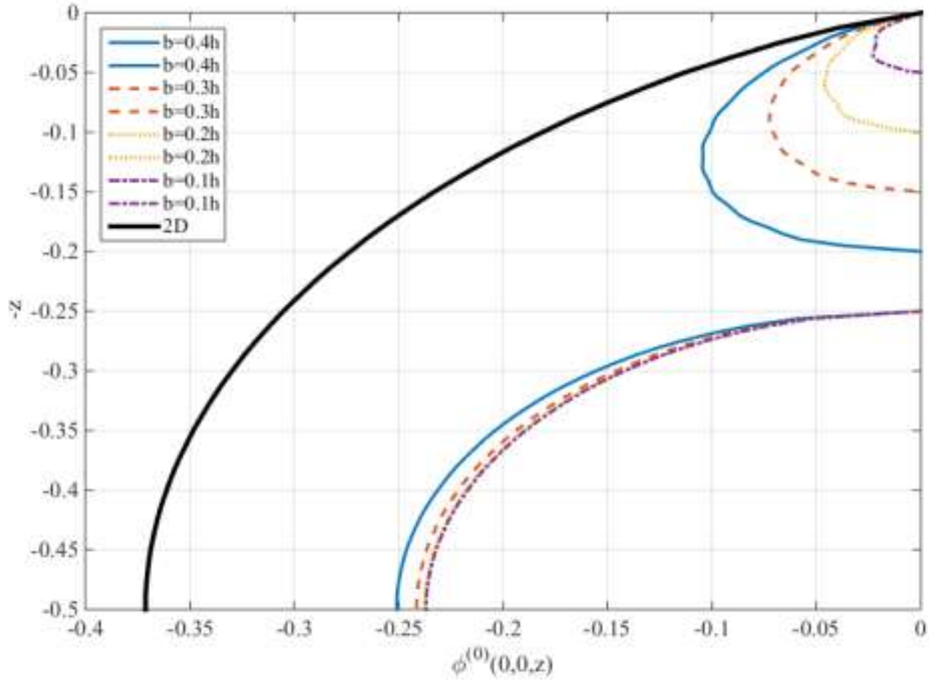

Fig. 4 The leading order potential ‰ ؟ πἰπἰ ἀ for a fixed lower edge ὤ j Ώ سى 0.5 and variable position of the upper edge ὤ7Ώ. The aspect ratio of the plate is Ώ سى Ό j ΰ سى 0.5.

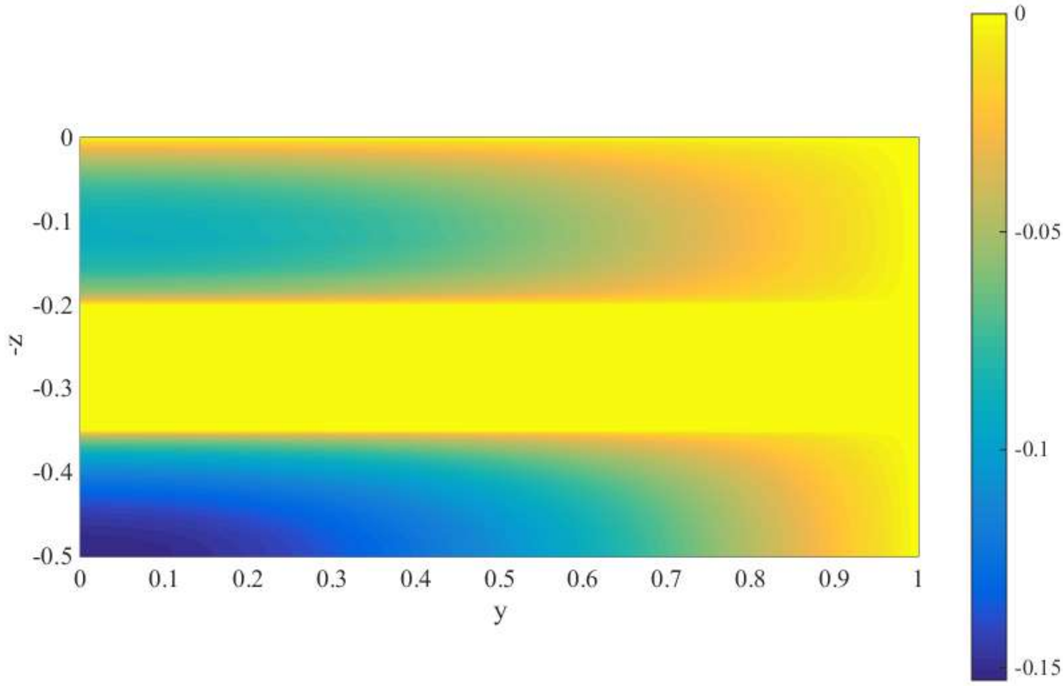

Fig. 5 The leading order potential ‰ ؟ πἰώἰ ἀ for lower edge ὤ j Ώ سى 0.7 and upper edge ὤ j Ώ سى 0.4. The aspect ratio of the plate is Ώ سى Ό j ΰ سى 0.5.

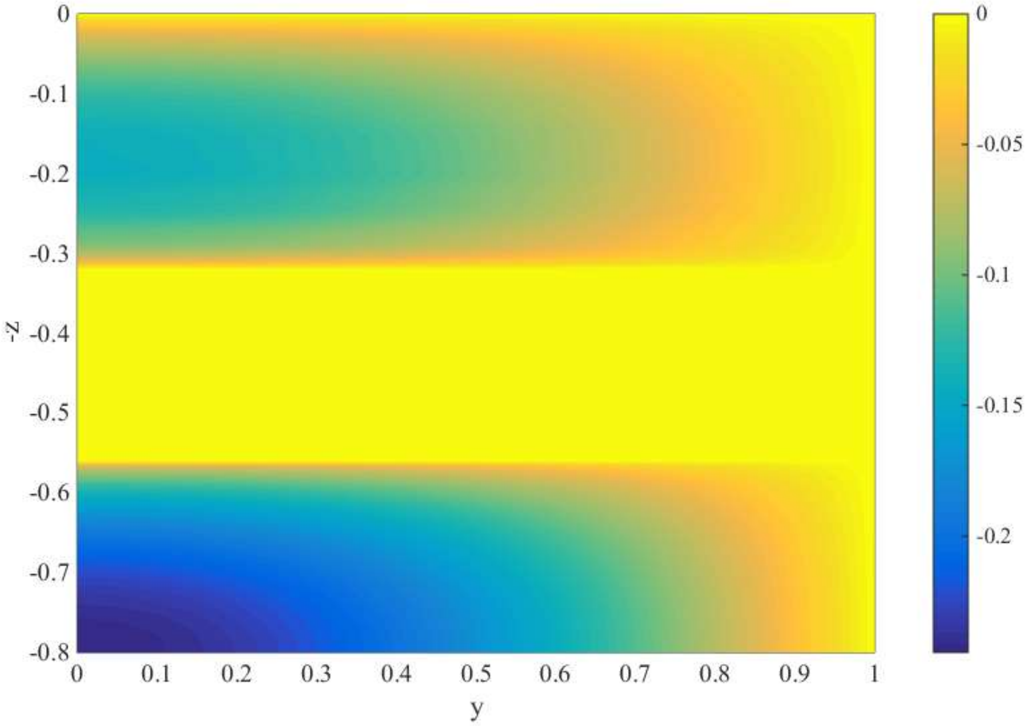

Fig. 6 The leading order potential ‰ ؟ πἡώἡᾳ for lower edge ὤ j ῑΩ سي 0.7 and upper edge ῶ j ῑΩ سي 0.4. The aspect ratio of the plate is ῑΩ سي ῑΟ j ΰ سي 0.8.

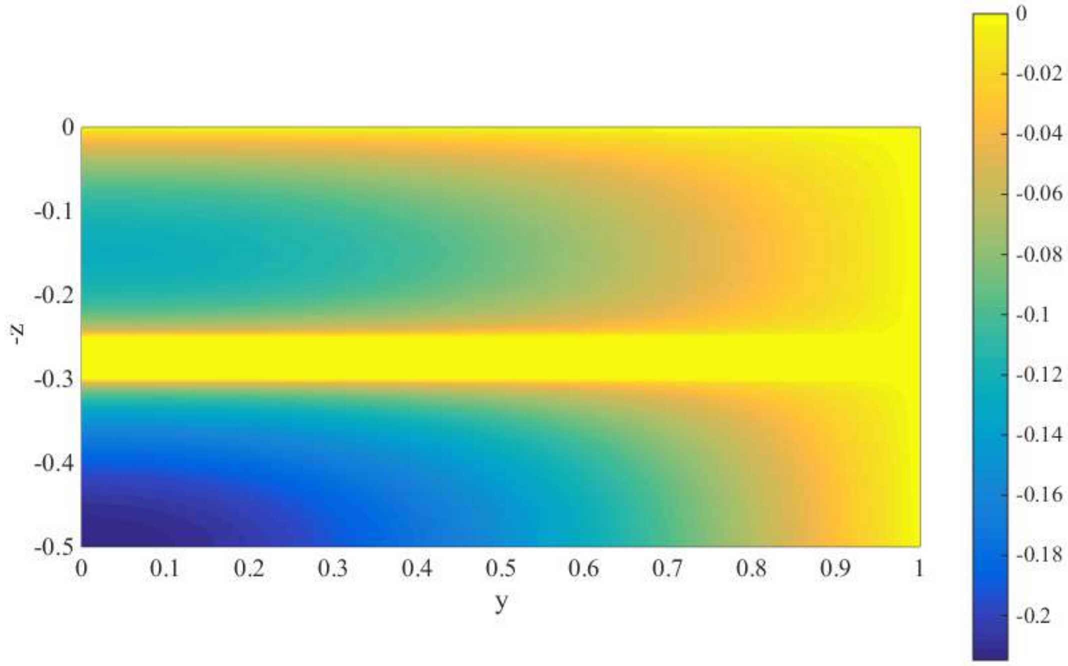

Fig. 7 The leading order potential ‰ ؟ πἡώἡᾳ for lower edge ὤ j ῑΩ سي 0.6 and upper edge ῶ j ῑΩ سي 0.5. The aspect ratio of the plate is ῑΩ سي ῑΟ j ΰ سي 0.5.

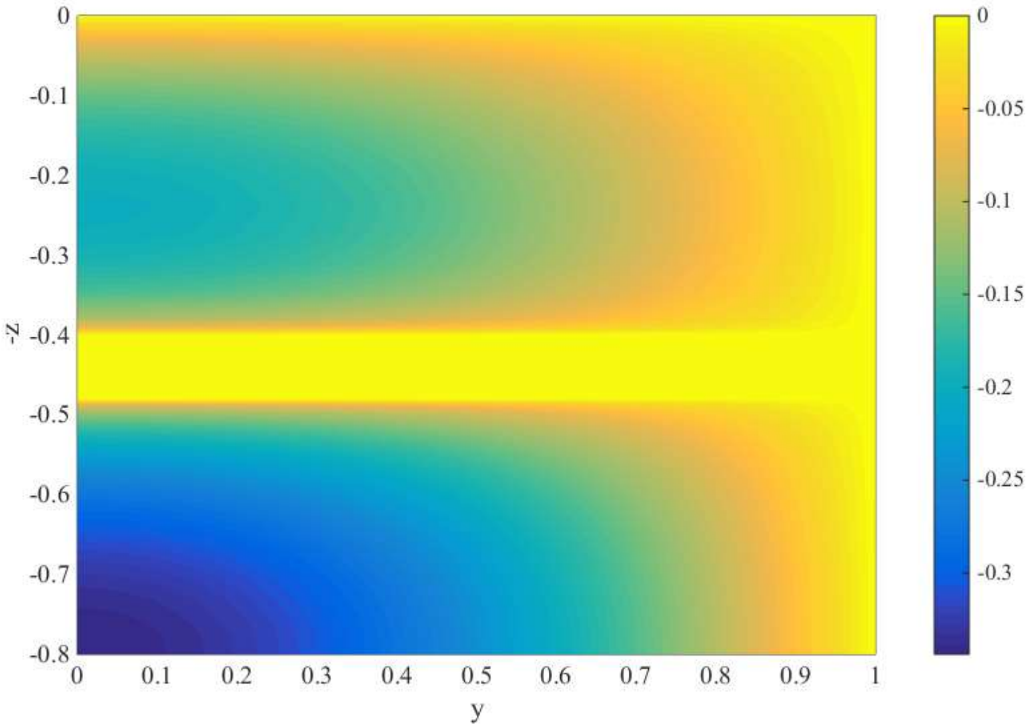

Fig. 8 The leading order potential $\Phi_0(y,z)$ for lower edge $c_1 = 0.6$ and upper edge $c_2 = 0.5$. The aspect ratio of the plate is $\beta = b/a = 0.8$.

The first-order potential is shown in Figs. 9-13. The aspect ratios, the dimensions and the locations of the open areas are defined in the figure captions. The cases examined in the contour plots of Figs. 10-13 are the same as those depicted in Figs. 5-8. As far as the first-order problem is concerned it is immediately apparent that the velocity potential does not comply with an explicit rule as regards its variation in the transverse direction y. Clearly the potential is zero throughout the surface of the open area as well as at the vertical edges of the plate. Fig. 9 depicts snapshots of the potential in both solid sections of the plate in 41 equally spaced points between $-1 \le y \le 1$. The first-order component exhibits vertically a type of parabolic variation on the upper solid section while in the lower section the potential starts from a maximum at the flat bottom and monotonically decreases to zero at the first horizontal edge from the bottom. The types of variations in y (or in x) cannot be explicitly defined as they are incorporated into the expansion coefficients of the triple trigonometrical series (and accordingly into the expansion coefficients of the integral equations).

The behaviour of the first-order velocity potential is better shown in the contour plots of Figs. 10-13. It is interesting to observe that the first-order component (which describes explicitly 3D effects) is relatively small at the centreline of the plate in both solid sections of it (note that the leading order component has maxima on the centreline). Widening the gap causes a decrease of potential in both sections, while for larger aspect ratios the magnitudes of the potential are increased. The most interesting characteristic of the first-order component is that the maximum potential occurs far from the centre line and close to the vertical edges. The positions of maxima on either side of $y = 0$, are the same for both solid sections and are detected at about $y = \pm 0.$[illegible]. Those findings clearly characterise the influence of the 3D effects. Indeed, these are important near the edges of the plate. For the higher aspect ratio case, the 3D effects due to the first-order potential appear to be more concentrated. In any event, the values of $\Phi_1(y,z)$ are much smaller than $\Phi_0(y,z)$ meaning that, as expected, the phenomenon is dominated by the leading order term.

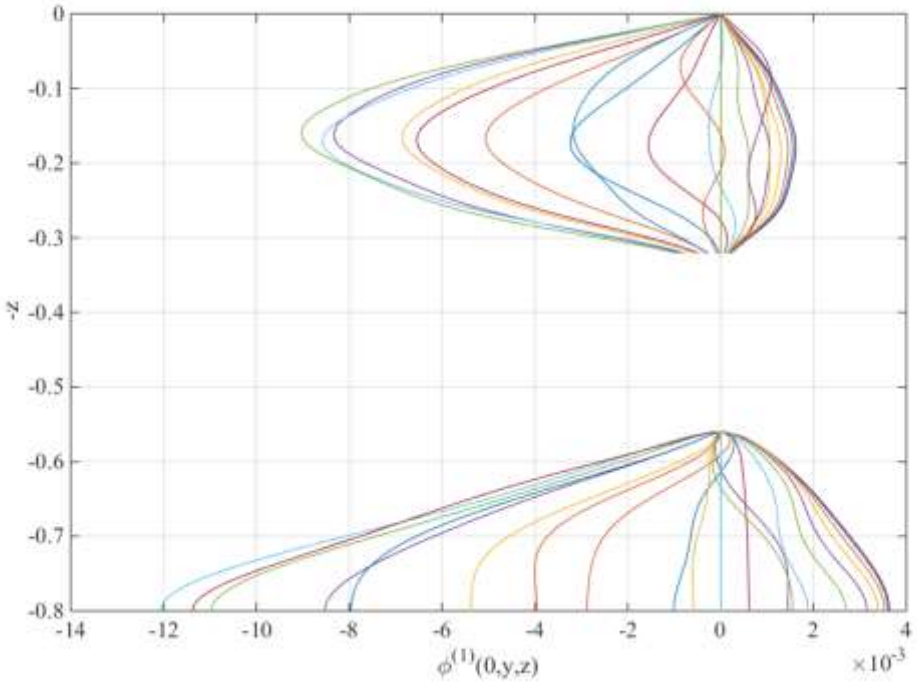

Fig. 9 The first-order potential ‰ ° πℓώℓφ for lower edge ώ j ΄Ω سي 0.7 and upper edge ω̃ j ΄Ω سي 0.4. The aspect ratio of the plate is ΄Ω سي ΄O j Ü سي 0.8.

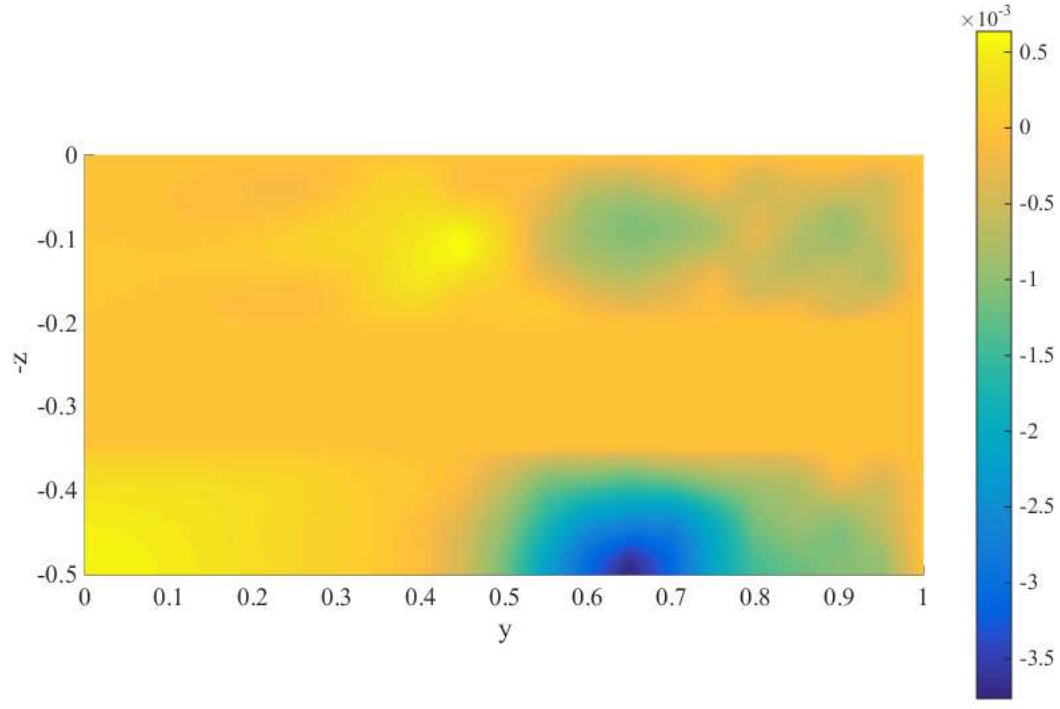

Fig. 10 The first-order potential ‰ ° πℓώℓφ for lower edge ώ j ΄Ω سي 0.7 and upper edge ω̃ j ΄Ω سي 0.4. The aspect ratio of the plate is ΄Ω سي ΄O j Ü سي 0.5.

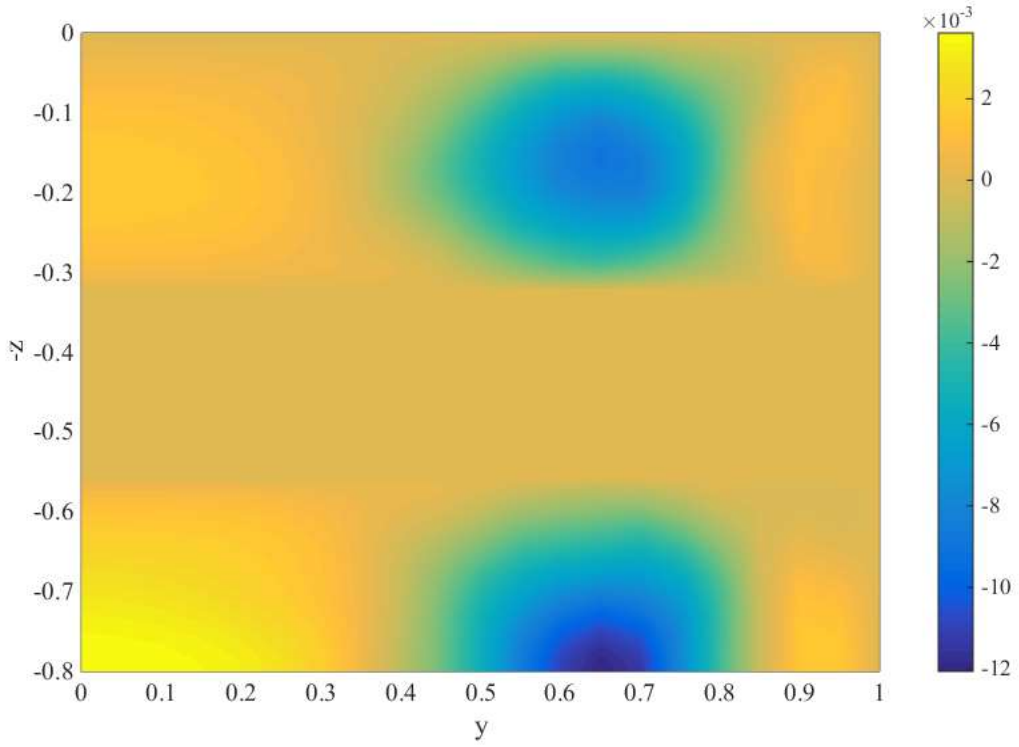

Fig. 11 The first-order potential ‰ ° πℏώℏά for lower edge ώ j ΅ سي 0.7 and upper edge ΰ j ΅ سي 0.4. The aspect ratio of the plate is ΅ سي ΅Ο j ü سي 0.8.

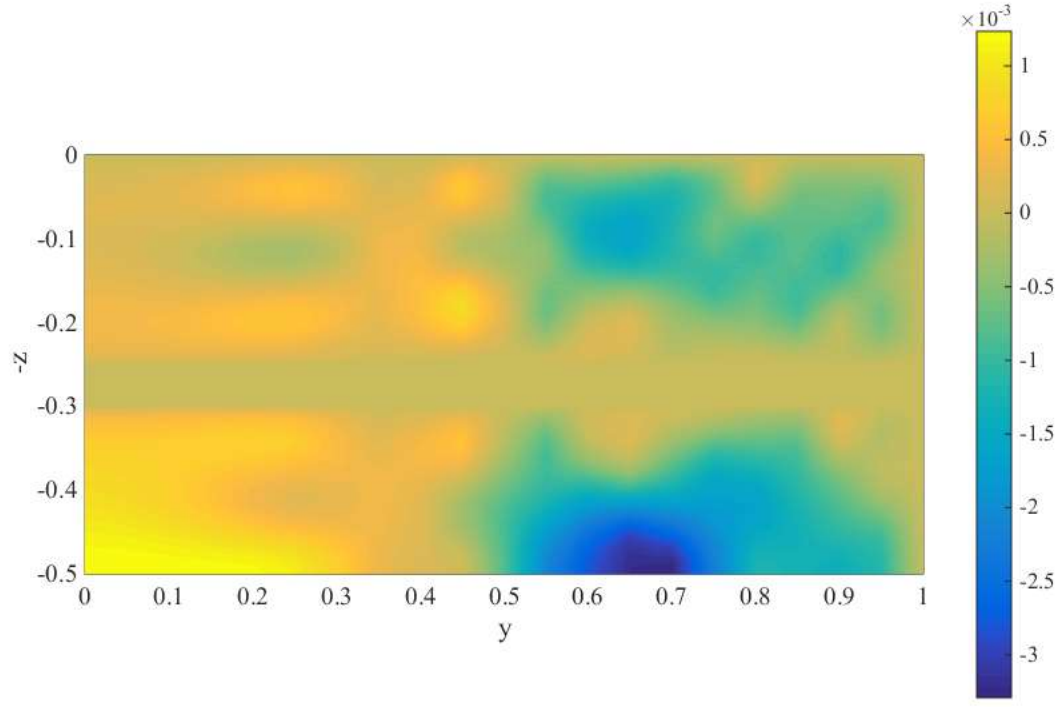

Fig. 12 The leading order potential ‰ ° πℏώℏά for lower edge ώ j ΅ سي 0.6 and upper edge ΰ j ΅ سي 0.5. The aspect ratio of the plate is ΅ سي ΅Ο j ü سي 0.5.

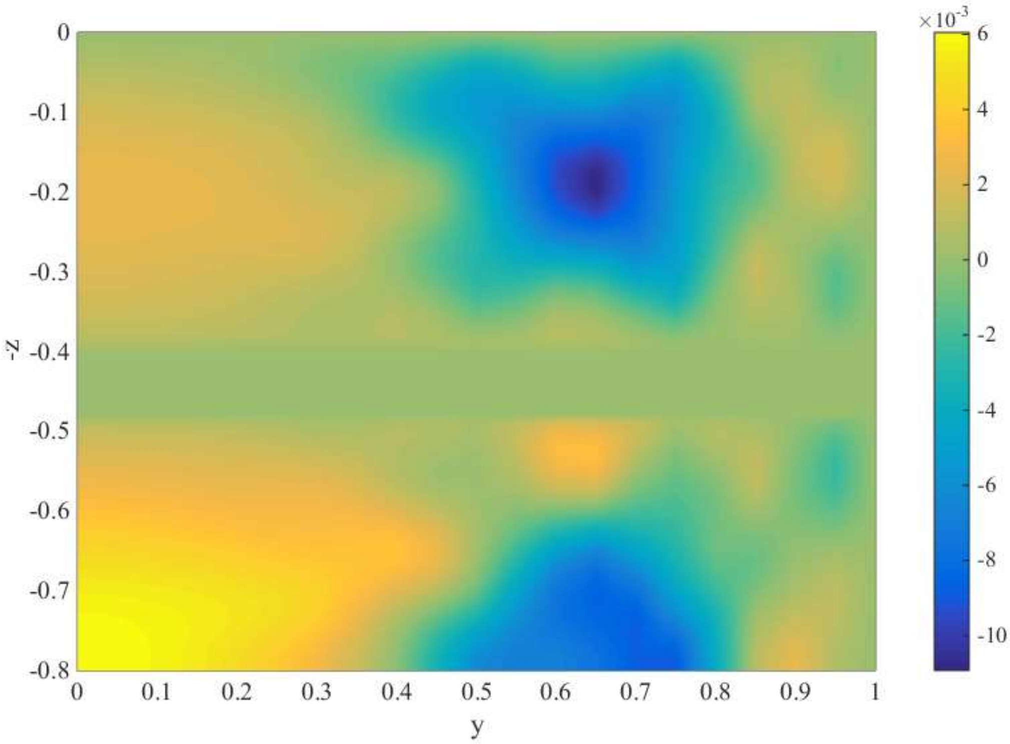

Fig. 13 The leading order potential $\phi_0(0,y,z)$ for lower edge $z = -0.6$ and upper edge $z = -0.5$. The aspect ratio of the plate is $= 0.8$.

8.2 Pressure-impulse

The phenomenon of hydrodynamic impact which involves a brief collision between a volume of liquid and a rigid body is better quantified by the so-called *Pressure-Impulse*, which is calculated by the short-lived pressures generated by the impact. According to Bagnold [43], the pressure-impulse is approximately constant (among repetitions of waves) at a fixed point on the impacted wall, although the peak pressures change unpredictably from any one impact to the next. Also, in contrast to the unpredictable behaviour of the peak pressures the pressure-impulse is well behaved, and accordingly is a better mathematical and physical quantity to model the impact phenomenon than the peak pressures [44].

Pressure-impulse has been mainly used to model flows induced instantaneously from rest, e.g. the impact of a rigid body striking the surface of still water [45-49]. Pressure-impulse theory, applied to the changes in a moving liquid domain that collides with a fixed structure, was introduced by Cooker and Peregrine [50]. Lamb [51] defines the pressure-impulse as

$$P(x,y,z) = \int_{t_b}^{t_a} p(x,y,z,t)\,dt \tag{92}$$

where the pressure $p(x,y,z,t) = -\rho\,\partial_t\phi(x,y,z,t)$, ρ is the water density and Δt is the short duration of the impact. Accordingly, $P(x,y,z) = -\rho\,\phi(x,y,z)$, where $\phi(x,y,z)$ is the change in the velocity potential induced by the impact. The total impulse is thus obtained by integrating the impulsive pressures oven the total impacted area at $x = 0$. Here, the total impulse, in normalized form, is given by

̓0 ̒Ω سي طي عجم عجم ‰ πἧ ώἧ ἀ̣ ἽΩώἽΩἀ̣ϑ (93)

where ̓0 ̒Ω also depends on the parameters ὥ and ῷ.

The scale of the total impulse is ”ὠϋ˥. The split in the potential suggests the split of the total impulse as well. Thus substituting Eqs. (90) and (91) into Eq. (93) and performing the integrations we obtain the following expressions of the total impulse in the leading and the first-order:

̓0 ̒Ω سي طي ̒Ω / ς“ ... (94)

̓0 ̒Ω سي طي ̒Ω / ς“˥ ... (95)

Results for the total impulse for ̒Ω سي πϑυ and 0.8 are shown in Figs. 14 and 15. Each figure contains both orders, while the total impulses are depicted as functions of ῷ/̒Ω for several values of ὥ/̒Ω. The impulse at leading order is decreased from small to large openings. The decrease however is relatively smooth following a curved path while the total impulse at leading order tends to an asymptotic constant as the height of the upper section obtains very small values.

The first-order component of the total impulse is more interesting. It starts from zero for wide openings while for the small aspect ratio case exhibits a maximum which however does not coincide with the case of narrow opening. For the large aspect ratio case, that maximum disappears. Nevertheless, the first-order total impulse is decreased as the opening practically vanishes. In this specific case the total impulse becomes negative. Finally, it can be safely concluded that the leading order total impulse is the dominant component as the first-order counterpart is negligible compared to the former.

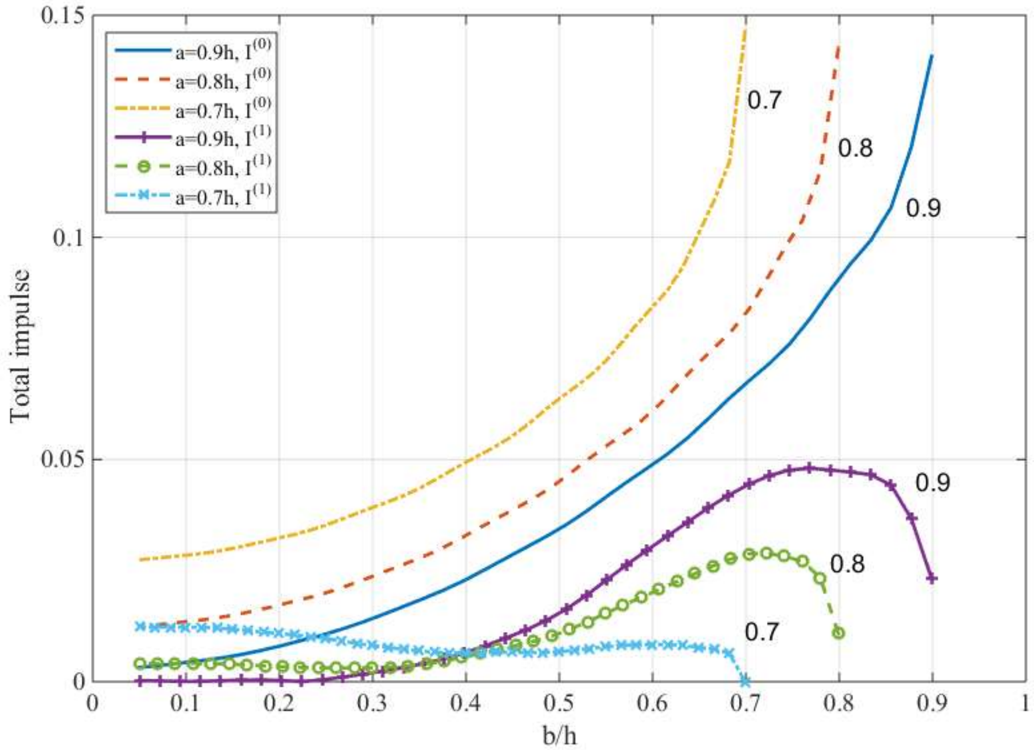

Fig. 14 Total impulses ͘ ؟ and ͘ ° as functions of ώ̃Ϳ͘Ω for several values of ώ̈Ϳ͘Ω. The aspect ratio of the plate is ͘Ω سي ͘Oϳϋ سي 0.5. For display purposes the total impulse at first-order has been multiplied by 50. Each curve has a right-end terminal point because ώ̃ حى ώ̈.

9 Conclusions

This study dealt with the 3D hydrodynamic impact problem on a vertical plate with a rectangular opening due to the impact of a steep wave. The solution method employed linear potential theory while the hydrodynamic problem was formulated as a boundary value problem of mixed type. The model equations defined two MBVPs for the two directions of the plate. The first MBVP was tackled assimilating the plate as a degenerate elliptical cylinder with negligible semi-minor axis. That allows the explicit satisfaction of the Dirichlet conditions of the change in the velocity potential (due to the brief impact) beyond the edges of the plate in the horizontal direction. Accordingly, the Neumann and the Dirichlet conditions on the solid parts of the plate and its opening, respectively, defined a new MBVP in the vertical direction involving triple trigonometrical series.

To achieve a solution for the latter MBVP, initially a perturbation technique was employed that defined components at various orders. The modified triple trigonometrical series MBVP was treated using a novel methodology that determined expressions in the form of triple integral equations. The sought solution was achieved by reducing the triple integral equations to dual trigonometrical series.

We presented results for the velocity potential that concerned both the leading order and the first-order components. As expected, the former was found to be much larger than the latter. The dominant leading order velocity potentials exhibited smooth variations both horizontally and vertically. It was also found that the existence of an opening along the plate‟s height, even when very small causes a drastic reduction of the change in the velocity potential due to the hydrodynamic impact. An increase in the plate‟s aspect ratio leads to an increase in the magnitude of the potential. The contour lines of the velocity potential were found to be elliptical in the upper solid section of the plate while their geometry on the lower section resembles half-ellipses. The maxima of the leading order component always occurred along the plate‟s centreline. In contrast, the first-order potential that is dominated by

the 3D effects was zero on the centreline and its maxima were concentrated close to the edges of the plate in the form of concentric circles on the upper solid section and semi-circles in the lower section.

Finally, pressure impulse theory was employed to evaluate the total impulse on the structure due to the wave at the instant of impact. In connection with pressure impulse, it was found that the leading order pressure impulse is reduced by widening the opening. In contrast, the significantly smaller first-order pressure impulse exhibits a complicated variation, while for very small openings it becomes negative.

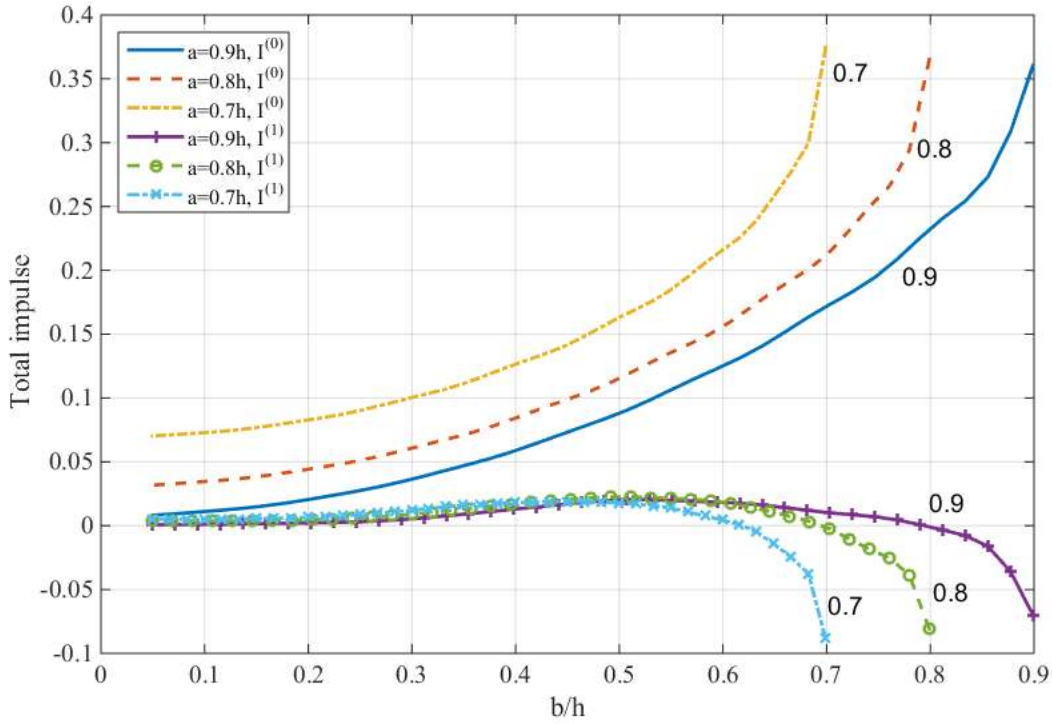

Fig. 15 Total impulses ϑ ϕ and ϑ ° as functions of ώ⁄Ω for several values of ώ⁄Ω. The aspect ratio of the plate is Ω سٍ Ο j ϑ سٍ 0.8. For display purposes the total impulse at first-order has been multiplied by 20. Each curve has a right-end terminal point because ώ حى ώ.

Acknowledgements. The authors are grateful to the EU Marie Curie Intra European Fellowship project SAFEMILLS "Increasing Safety of Offshore Wind Turbines Operation: Study of the violent wave loads" under grant 622617.

References

[1] Korobkin AA, Scolan Y-M. Three-dimensional theory of water impact. Part 2. Linearized Wagner problem. Journal of Fluid Mechanics 2006; 549:343-373.

[2] Scolan Y-M, Korobkin AA. Three-dimensional theory of water impact. Part 1. Inverse Wagner problem. Journal of Fluid Mechanics 2001; 440:293-326.

[3] Scolan Y-M. Hydrodynamic impact of an elliptic paraboloid on cylindrical waves. Journal of Fluids and Structures 2014; 48:470-486.

[4] Peregrine DH. Water-wave impact on walls. Annual Review of Fluid Mechanics 2003; 35:23-43.

[5] Wood D, Peregrine DH, Bruce T. Wave impact on a wall using pressure-impulse theory: I: Trapped air. Journal of Waterway, Port, Coastal and Ocean Engineering 2000; 126:182-190.

[6] Wood D, Peregrine DH. Wave impact on a wall using pressure-impulse theory: II: Porous berm. Journal of Waterway, Port, Coastal and Ocean Engineering 2000; 126:191-195.

[7] Bullock GN, Obharai C, Peregrine DH, Bredmose H. Violent breaking wave impacts. Part 1: Results from large-scale regular wave tests on vertical and sloping walls. Coastal Engineering 2007; 54:602-617.

[8] Bredmose H, Peregrine DH, Bullock GN. Violent breaking wave impacts. Part 2: modelling the effect of air. Journal of Fluid Mechanics 2009; 641:389-430.

[9] Bredmose H, Bullock GN, Hogg AJ. Violent breaking wave impacts. Part 3. Effects of scale and aeration. Journal of Fluid Mechanics 2015; 765:82-113.

[10] Cooker MJ. A theory for the impact of a wave breaking onto a permeable barrier with jet generation. Journal of Engineering Mathematics 2013; 79:1-12.

[11] Cuomo G, Allsop W, Bruce T, Pearson J. Breaking wave loads at vertical seawalls and breakwaters. Coastal Engineering 2010; 57:424-439.

[12] Rafiee A, Dutykh D, Dias F. Numerical simulation of wave impact on a rigid wall using a two-phase compressible SPH method. Procedia IUTAM 2015; 18:123-137.

[13] Carratelli EP, Viccione G, Bovolin V. Free surface flow impact on a vertical wall: a numerical assessment. Theoretical and Computational Fluid Dynamics 2016; 30:403-414.

[14] Korobkin AA, Malenica Š. Steep wave impact onto elastic wall. Proc. 22nd International Workshop on Water Waves and Floating Bodies, Plitvice, Croatia 2007; 129-132.

[15] Noar NAZM, Greenhow M. Wave impacts on structures with rectangular geometries: Part 1 Seawalls. Applied Ocean Research 2015; 53:132-141.

[16] Korobkin AA. Non-classical boundary conditions in water-impact problems. IUTAM Symposium (ed. E. Kreuzer) 2008; 167-178.

[17] Kleefsman KMT, Fekken G, Veldman AEP, Iwanowski B, Buchner B. A Volume-of-Fluid based simulation method for wave impact problems. Journal of Computational Physics 2005; 206:363-393.

[18] Yang C, Lin B, Jiang C, Liu Y. Predicting near-field dam-break flow and impact force using a 3D model. Journal of Hydraulic Research 2010; 48:784-792.

[19] Gómez-Gesteira M, Dalrymple RA. Using a three-dimensional smoothed particle hydrodynamics method for wave impact on a tall structure. Journal of Waterway, Port, Coastal and Ocean Engineering 2004; 130:63-69.

[20] Cummins SJ, Silvester TB, Cleary PW. Three-dimensional wave impact on a rigid structure using smoothed particle hydrodynamics. International Journal for Numerical Methods in Fluids 2012; 68:1471-1496.

[21] Chatjigeorgiou IK, Korobkin AA, Cooker MJ. Three-dimensional steep wave impact onto a vertical plate of finite width. Proc 31st International Workshop on Water Waves and Floating Bodies, Plymouth, MI, USA 2016; 9-12.

[22] Abramowitz M, Stegun IA. Handbook of mathematical functions. New York: Dover Publications Inc.; 1970.

[23] King AC, Needham DJ. Initial development of a jet caused by fluid, body and free-surface interaction. Part 1. A uniformly accelerating plate. Journal of Fluid Mechanics 1994; 268:89-101.

[24] Sharma K, Marin M. Effect of distinct conductive and thermodynamic temperatures on the reflection of plane waves in micropolar elastic half space. Scientific Bulletin UPB Series A 2013; 75:121-132.
[25] Marin M. On weak solutions in elasticity of dipolar bodies with voids. Journal of Computational and Applied Mathematics 1997; 82: 291-297.
[26] Marin M. Harmonic vibrations in thermoelasticity of microstretch materials. Journal of Vibration and Acoustics 2010; 132: 044501.
[27] Shepherd WM. On trigonometrical series with mixed conditions. Proc. London Mathematical Society 1938; 43:366-375.
[28] Tranter CJ. Dual trigonometrical series. Glasgow Mathematical Journal 1959; 4:49-57.
[29] Tranter CJ. A further note on dual trigonometrical series. Glasgow Mathematical Journal 1960 4: 198-200.
[30] Tranter CJ. An improved method for dual trigonometrical series. Glasgow Mathematical Journal 1964; 6:136-140.
[31] Srivastav RP. Dual series relations. III. Dual relations involving trigonometric series. Proc. Royal Society Edinburgh 1963; 66:173-184.
[32] Sneddon IN. Mixed boundary value problems in potential theory. Amsterdam: North Holland Publishing Company; 1966.
[33] Fabrikant VI. Mixed boundary value problems of potential theory and their applications in engineering. Dordrecht: Kluer Academic Publishers; 1991.
[34] Duffy DG. Mixed boundary value problems. Boca Raton, FL: Chapman & Hall/CRC; 2008.
[35] Tranter CJ. Some triple trigonometrical series. Glasgow Mathematical Journal 1969; 10:121-125.
[36] Kerr G, Melrose G, Tweed J. Some triple sine series. Applied Mathematics Letters 1994; 7:33-36.
[37] Williams WE. Note on the reduction of dual and triple series equations to dual and triple integral equations. Proc. Cambridge Philosophical Society 1963; 59:731-734.
[38] Watson GN. A treatise on the theory of Bessel functions. Cambridge: Cambridge University Press; 1944.
[39] Gradshteyn IS, Ryzhik IM. Table of integrals, series and products. 7th edition London: Elsevier Academic Press; 2007.
[40] Titchmarsh EC. Introduction to the theory of Fourier integrals. 2nd edition Oxford: Clarendon Press; 1948.
[41] Tranter CJ (1960) Some triple integral equations. Glasgow Mathematical Journal 4:200-203.
[42] Magnus W, Oberhettinger F. Formulas and theorems for the special functions of mathematical physics. New York: Chelsea; 1949.
[43] Bagnold RA. Interim report on wave pressure research. Journal of Institution of Civil Engineers 1939; 12:201-226.
[44] Richert G. Experimental investigation of shock pressures against breakwaters. Proc. 11th Conference on Coastal Engineering, ASCE 1968; 945-973.
[45] Batchelor GK. An introduction to fluid dynamics. Cambridge: Cambridge University Press; 1973.
[46] Cointe R, Armand J-L. Hydrodynamic impact analysis of a cylinder. Transactions ASME, Journal of Offshore Mechanics and Arctic Engineering 1987; 109:237-243.
[47] Cointe R. Two-dimensional water-solid impact. Transactions ASME, Journal of Offshore Mechanics and Arctic Engineering 1989; 111:1090-114.
[48] Howison SD, Ockendon JR, Wilson SK. A note on incompressible water entry problems at small dead-rise angles. Journal of Fluid Mechanics 1991; 222:215-230.
[49] Wagner H. Über Stross- und Gleitvorgänge an der Oberfläche von Flüssigkeiten. Z. Angew. Math. Mech. 1932; 12:193-215. (English transl: Phenomena associated with impacts and sliding on liquid surfaces. NACA Translation 1366)
[50] Cooker MJ, Peregrine DH. Pressure-impulse theory for liquid impact problems. Journal of Fluid Mechanics 1995; 297:193-214.
[51] Lamb H. Hydrodynamics. 6th edition Cambridge: Cambridge University Press; 1932.

Graphical abstract

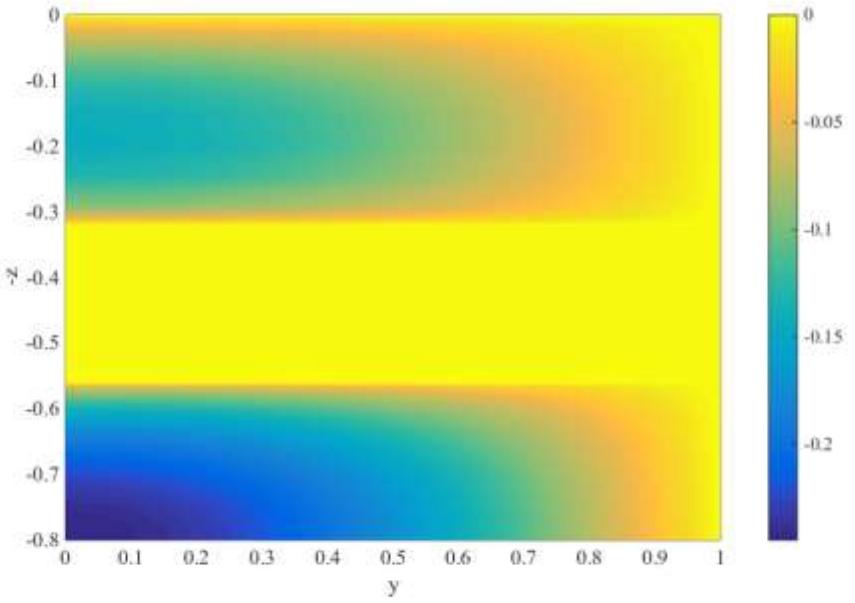

The leading order potential during the impact of a steep wave on a vertical plate with an open rectangular section

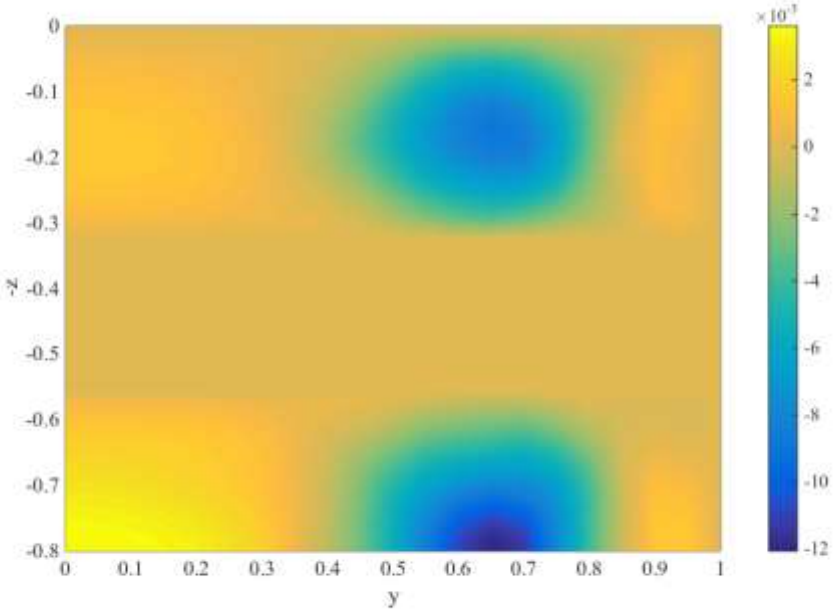

The first-order potential during the impact of a steep wave on a vertical plate with an open rectangular section